今までの地下(および水中,氷中)実験のまとめ

岡田論(ICRR)

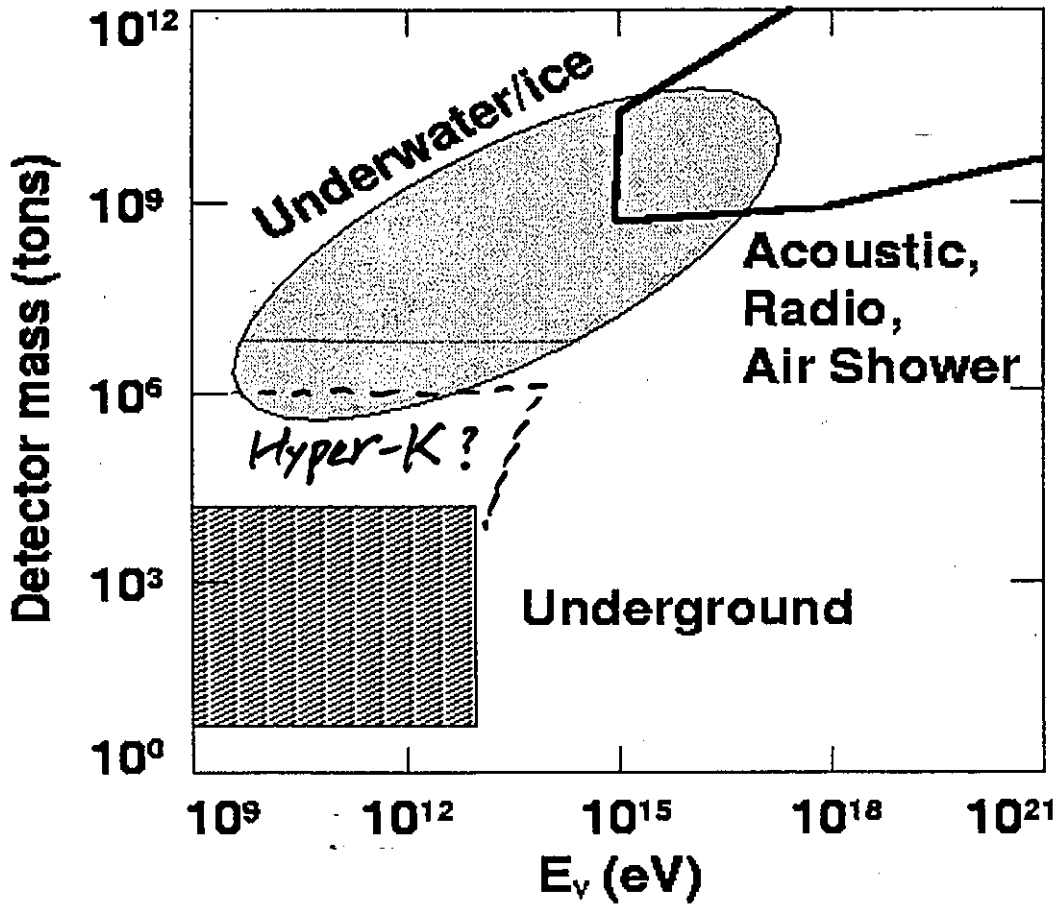

Figure 1. Domains of different detection techniques.
(from C. Spiering)

Underground Detectors

sensitive 領域明確
技術的大失敗少ない
(現場で行う)
大型化困難 → 比較的 low energy 狙う
(Protondecay, Monopole, Neutralino, SN, ⋮)

×	Nusex	1982 - 1988
	IMB	1982 - 1991
	Kamiokande	1983 - 1995
	SN1987A, solar ν	
×	Frejus	1984 - 1988
	Soudan2	1989 - (1993) -
–	MACRO	1991 - 2000
	Super-Kamiokande	1996 -
	ν oscillation	

Upward throughgoing muons → Heastro. ν

× up/down ≈ 1
– water Čerenkov

SK water. Čerenkov detector situated in a Zinc mine

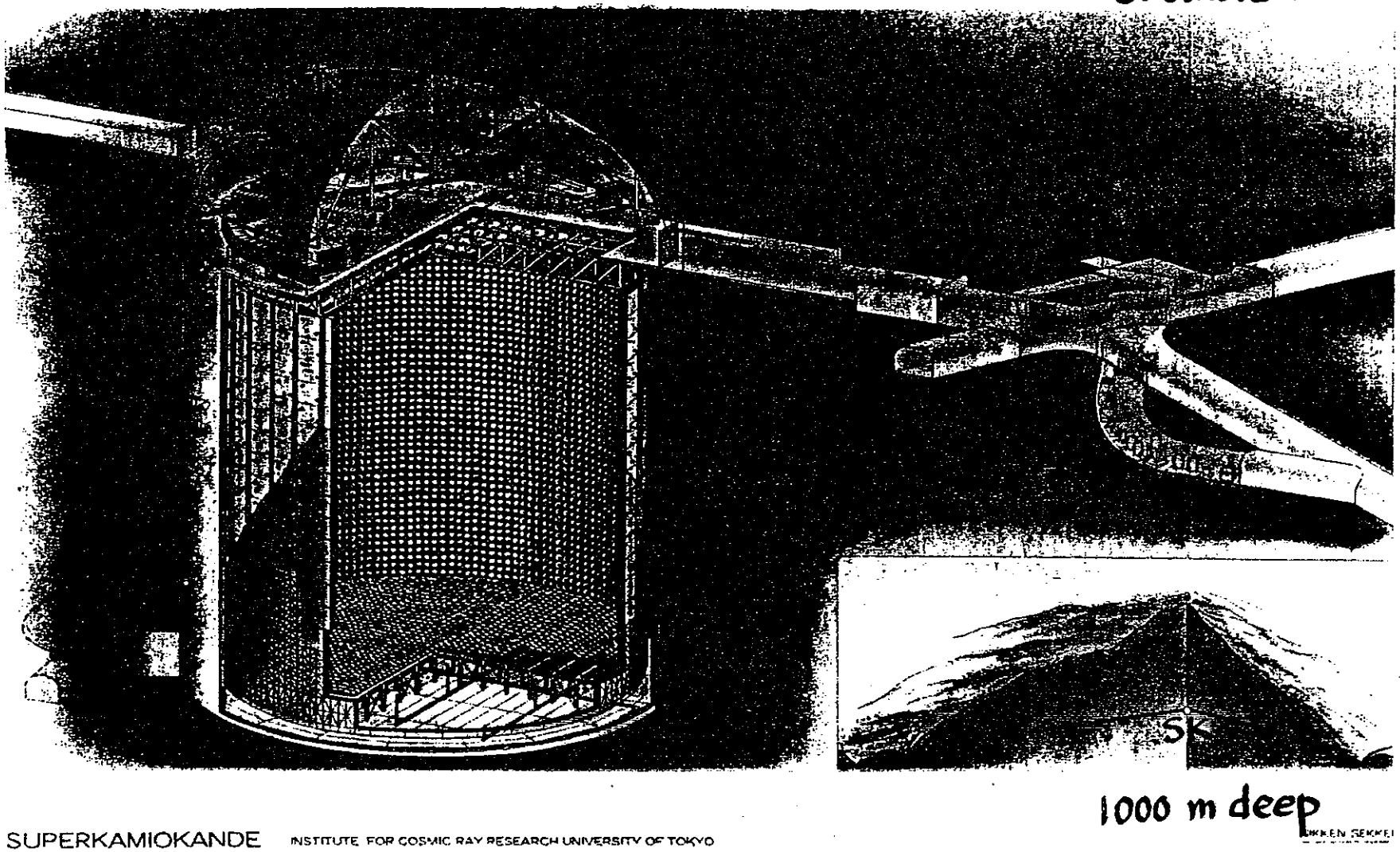

11,146 20' PMTs for inner detector

1,885 8' PMTs for outer "

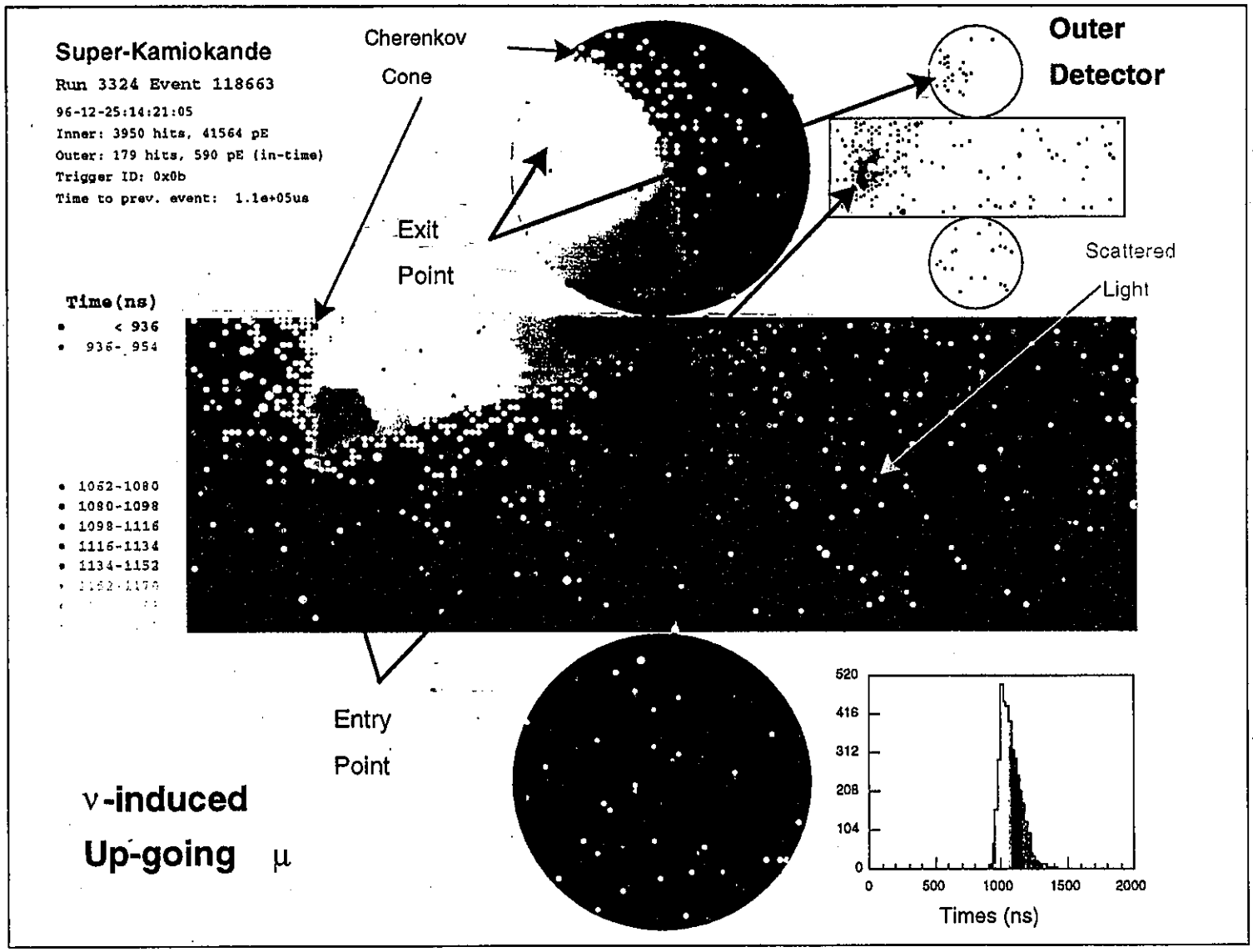
Super-Kamiokande
Run 3324 Event 118663
96-12-25:14:21:05
Inner: 3950 hits, 41564 pE
Outer: 179 hits, 590 pE (in-time)
Trigger ID: 0x0b
Time to prev. event: 1.1e+05us
Cherenkov
Cone
Outer
Detector
Exit
Point
Scattered
Light
Time(ns)
< 936
936- 954
1062-1080
1080-1098
1098-1116
1116-1134
1134-1152
Entry
Point
ν-induced
Up-going μ
520
416
312
208
104
0
0
500
1000
1500
2000
Times (ns)

THE MACRO DETECTOR

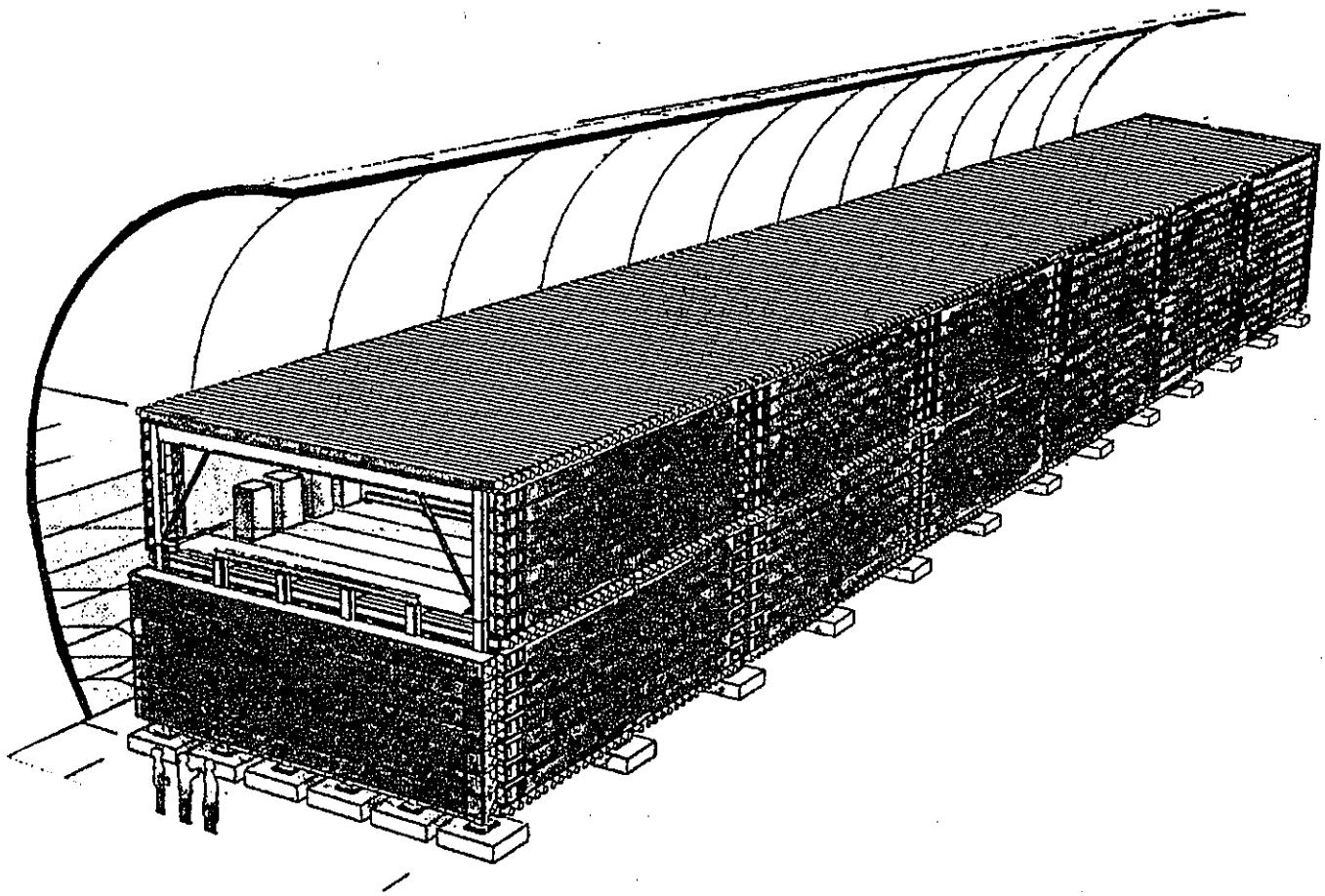

Overall view of the MACRO detector at Gran Sasso. It has dimensions of:

12 m horizontal
76.6 m in length
9.3 m height.

The detector is subdivided in 6 supermodules, with a lower and an upper part.

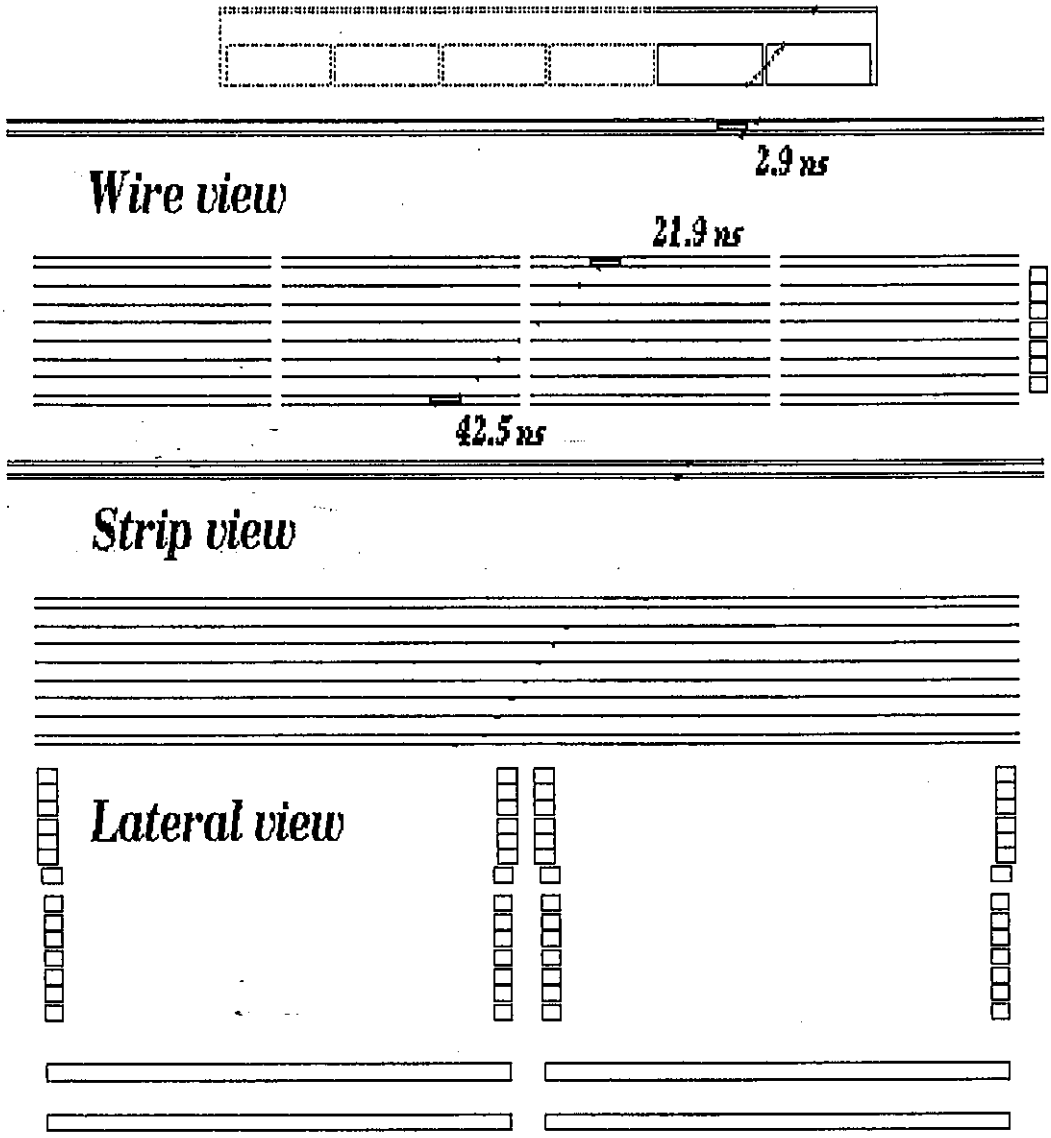

Fig. 3.– One upward-going muon produced by a neutrino interaction in the rock below the MACRO detector. The wire, strip and lateral views are shown and the times in nanoseconds are indicated near the scintillator counters hit by the track. The first hit counter corresponds to the larger time.

Zenith Angle Dist. of Observed Upward Through Going Muon Flux

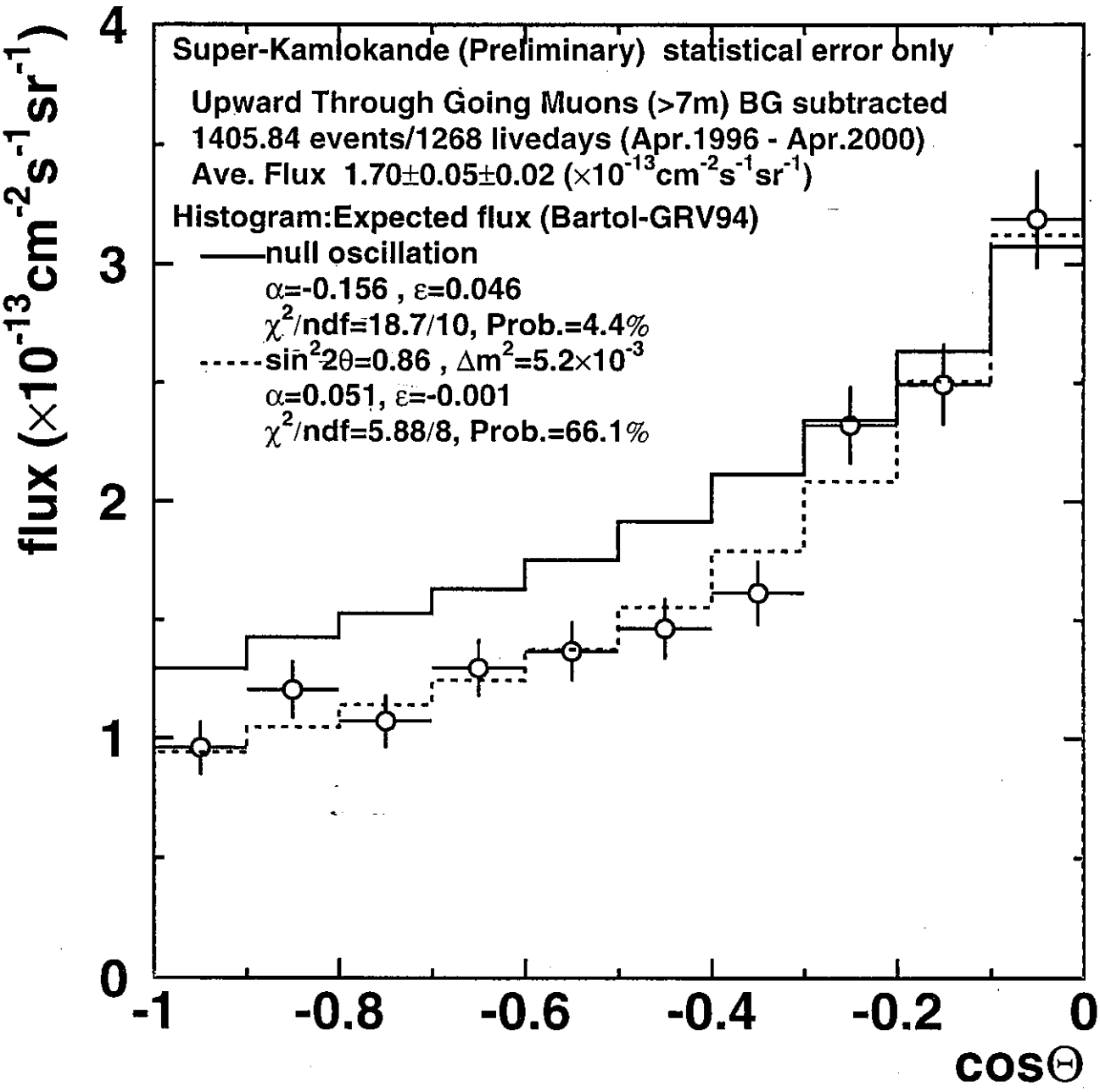

ZENITH DISTRIBUTION AND MONTECARLO PREDICTIONS FOR UPGOING MUONS

(Average ν_μ energy $\sim$ 100 GeV)

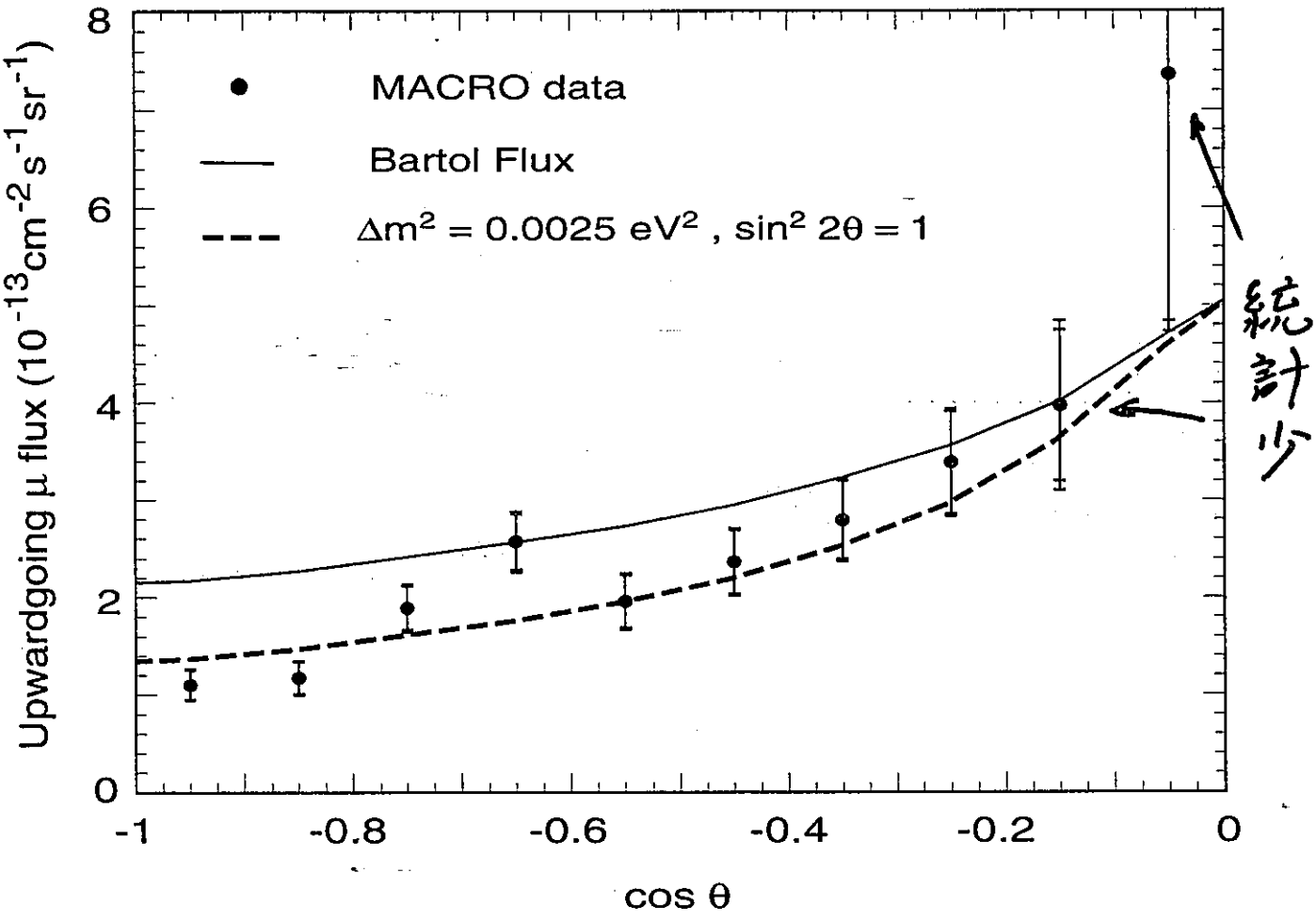

Zenith distribution of the flux of neutrino-induced upwardgoing muons with energy greater than 1 GeV for the data and for the MonteCarlo predictions. The solid curve shows the expectation for no oscillations and the shaded region shows the uncertainty in the expectation. The lower solid line shows the prediction for an oscillated flux with $\sin^2 2\theta = 1$ and $\Delta m^2 = 0.0025$ eV^2.

909 events in total (?)

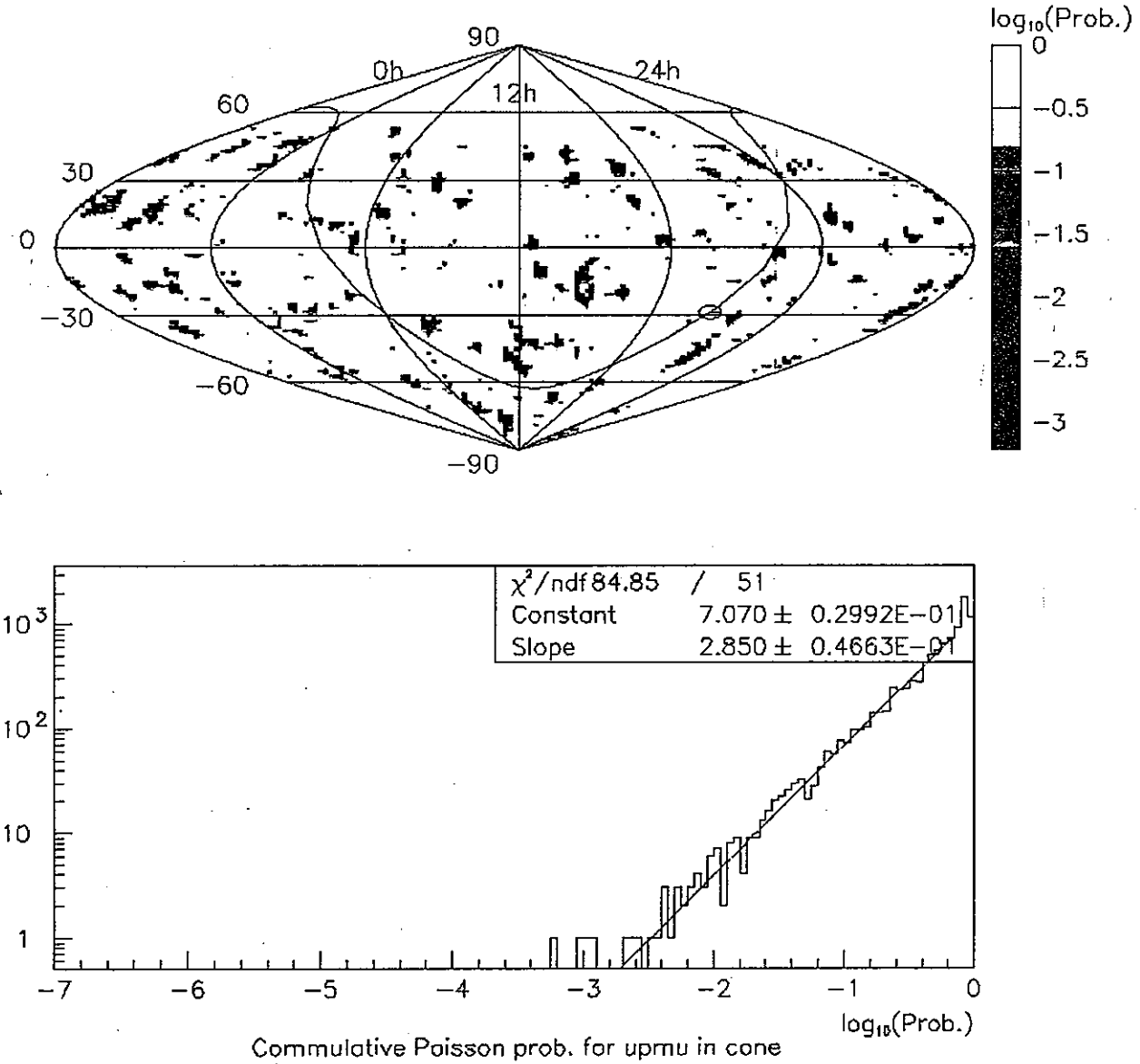

Super- K

Fig. 1. Top panel: cumulative Poisson probability sky map in an equatorial coordinate. An S-shaped line in the figure shows the Galactic plane and an ellipse on it indicates the Galactic Center. Declination region above 54° is not accessible with the Super-Kamiokande detector using UGM data.
Bottom panel: $\log_{10}$(probability) frequency distribution in the sky with a fit to an exponential function.

NEUTRINO ASTRONOMY WITH MACRO

Several astrophysical bodies are expected to yield very high energy neutrinos.

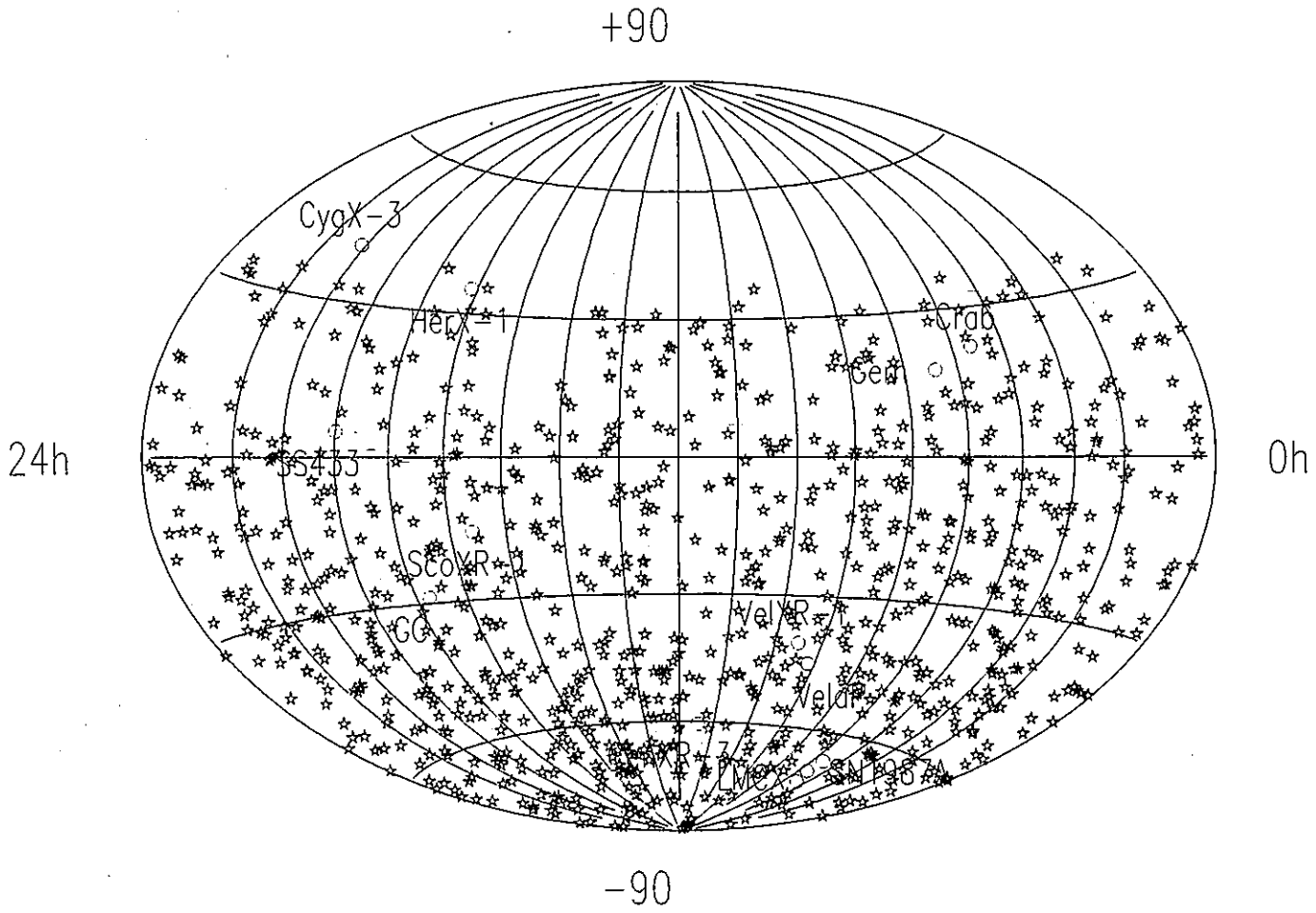

MACRO detects upgoing muons (with $E_\mu > 1$ GeV) from ν_μ interacting in the rock below the apparatus. The good angular resolution of MACRO allows to search for excesses of upgoing muons in narrow angular bins. No significant clustering of muons around specific directions is observed in a sky survey using 909 upgoing muons. The neutrino flux limits from specific sources are at the level of $\sim 10^{-14}$ cm^{-2}s^{-1}.

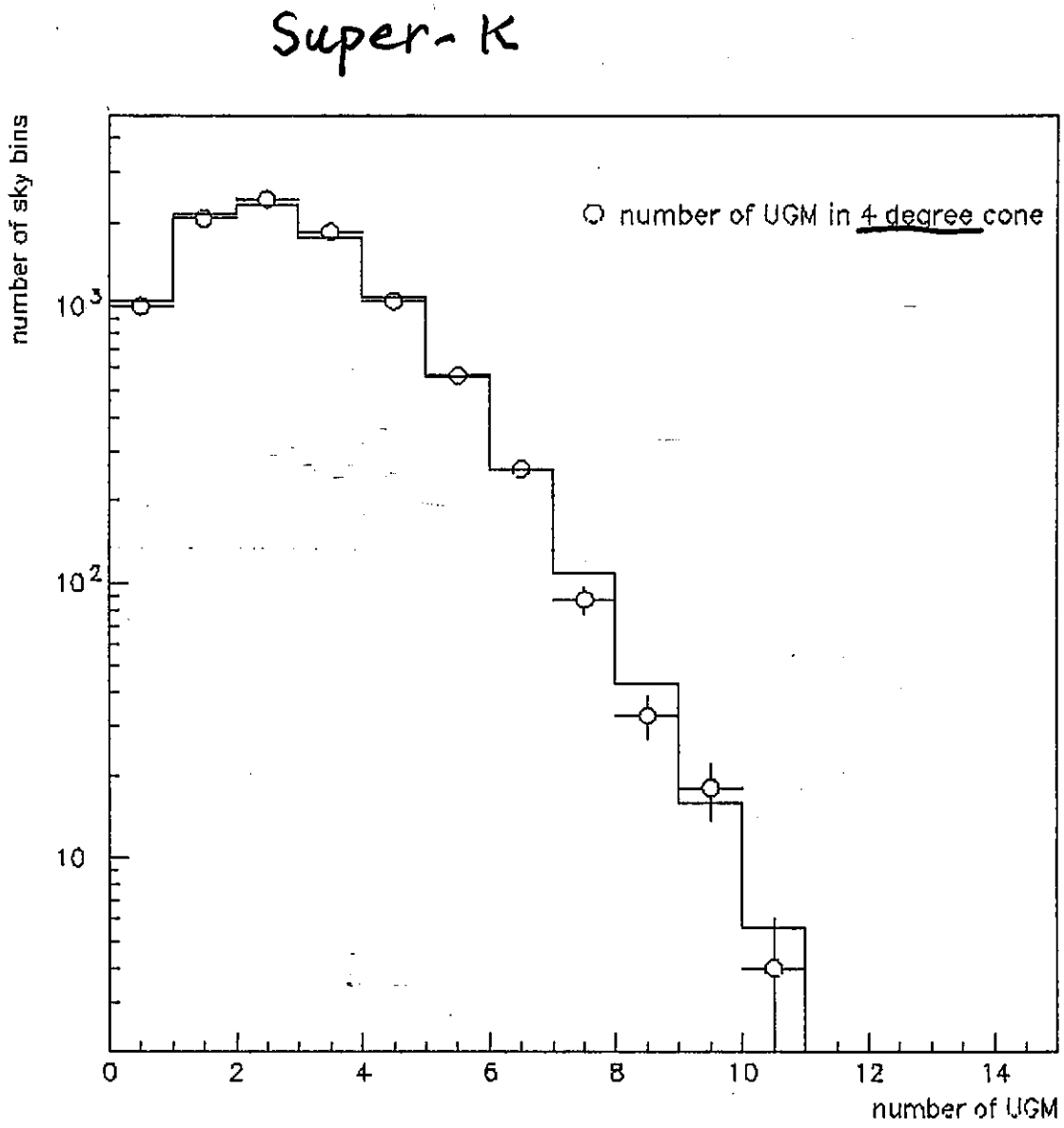

Fig. 2. UGM number distribution in the sky. The solid histogram in the figure shows expected distribution from noise obtained by "bootstrap method".

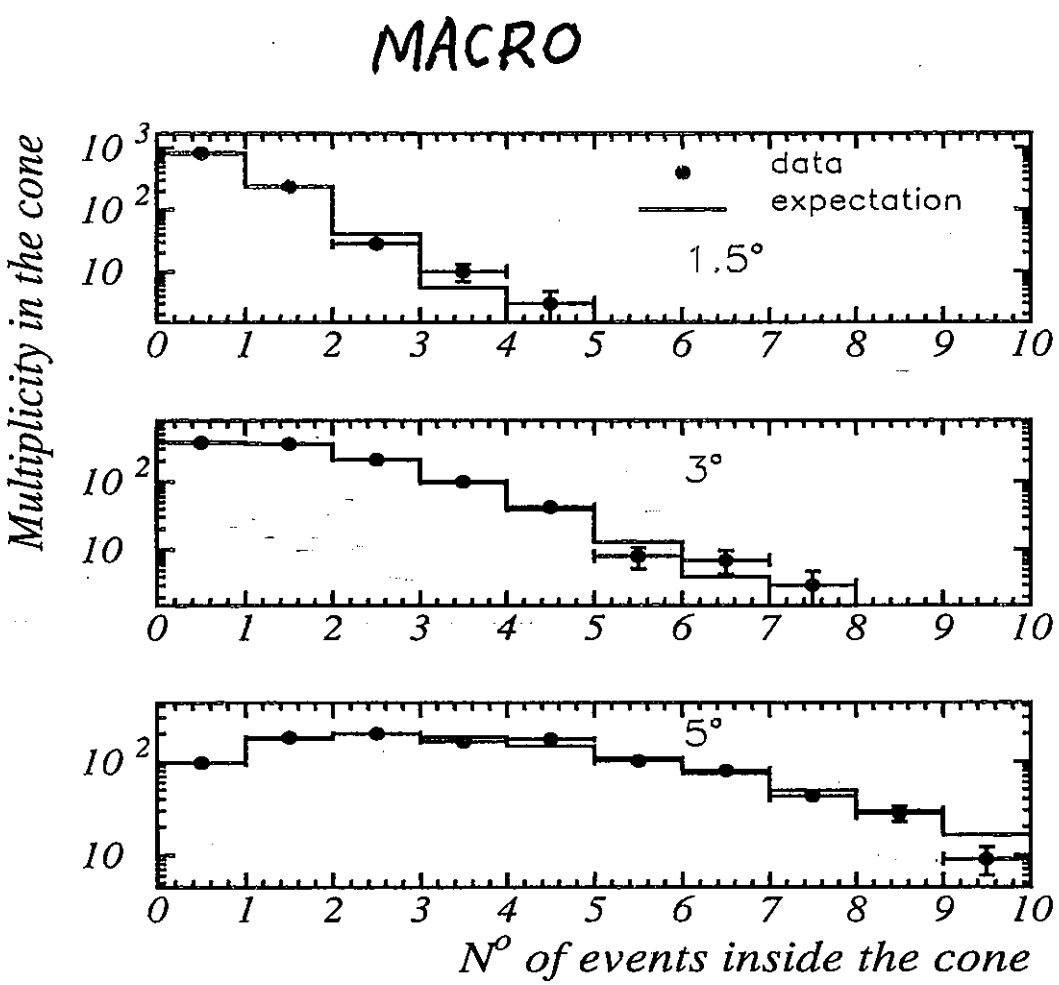

Fig. 10.— On the x axis there is the number of events falling in cones of half width 1.5°, 3°, 5° (from top to bottom plot) around the direction of any muon. The y axis depends on the total number of events considered. Black circles: data. Solid line: simulation.

Potential Source Name	UGM observed in 4^o cone	noise expected	Accept. (cm^2)	Flux Limit ($cm^{-2}s^{-1}$)
Cyg X-1	6	2.0	4.1×10^6	2.4×10^{-14}
Cyg X-3	1	1.8	3.5×10^6	1.0×10^{-14}
Her X-1	1	1.7	4.1×10^6	8.7×10^{-15}
Sco X-1	2	2.6	6.9×10^6	7.0×10^{-15}
Vela X-1	5	2.9	8.6×10^6	9.9×10^{-15}
Crab N.	0	1.8	5.1×10^6	4.1×10^{-15}
3C273	6	2.4	6.2×10^6	1.6×10^{-14}
Per A	1	1.9	3.4×10^6	1.1×10^{-14}
Vir A	1	1.7	5.7×10^6	6.3×10^{-15}
Coma cl.	2	1.7	4.7×10^6	1.0×10^{-14}
Gemminga	3	2.0	5.4×10^6	1.1×10^{-14}
Gal. C.	3	2.2	7.6×10^6	8.0×10^{-15}
Mrk 421	2	1.9	3.8×10^6	1.3×10^{-14}
Mrk 501	1	1.9	3.6×10^6	9.9×10^{-15}

Super-K

Table 1. Up going muon flux limit for various potential neutrino sources in the sky. $E_\mu \geq 1.6$ GeV

MACRO

Table 3. 90% c.l. neutrino induced μ-flux limits for the MACRO list of 42 sources. Corresponding limits on the neutrino flux are given in the last column. These limits are calculated for $\gamma = 2.1$ and for $E_\mu > 1$ GeV including the decrease in efficiency at very high energies. The reduction factors for a 3° half width cone are included. These limits include the effect of absorption of neutrinos in the Earth. The flux upper limits are calculated with the unified approach of Feldman & Cousins (69). B indicates the results of Baksan (26); I the results of IMB (24).

Source	δ (degrees)	Events in 3°	Backg. in 3°	ν induced μ-Flux Limits (10^{-14} cm^{-2} s^{-1})	Previous best μ limits (10^{-14} cm^{-2} s^{-1})	ν-Flux limits (10^{-6} cm^{-2} s^{-1})
SMC X-1	-73.5	3	2.1	0.62	-	1.18
LMCX-2	-72.0	0	2.0	0.15	-	0.33
LMCX-4	-69.5	0	2.0	0.15	0.36 B	0.29
SN1987A	-69.3	0	2.0	0.15	1.15 B	0.31
GX301-2	-62.7	2	1.8	0.53	-	1.10
Cen X-5	-62.2	2	1.7	0.55	-	1.04
GX304-1	-61.6	2	1.7	0.54	-	1.05
CENXR-3	-60.6	1	1.7	0.36	0.98 I	0.68
CirXR-1	-57.1	5	1.7	1.18	-	2.21
2U1637-53	-53.4	0	1.7	0.19	-	0.36
MX1608-53	-52.4	0	1.7	0.20	-	0.38
GX339-4	-48.8	6	1.7	1.62	-	3.00
ARA XR1	-45.6	3	1.6	1.00	-	1.87
VelaP	-45.2	1	1.5	0.51	0.78 I	0.94
GX346-7	-44.5	0	1.5	0.23	-	0.43
SN1006	-41.7	1	1.3	0.56	-	1.04
VelaXR-1	-40.5	0	1.3	0.26	0.45 B	0.55
2U1700-37	-37.8	1	1.3	0.58	-	1.08
L10	-37.0	2	1.1	0.91	-	1.72
SGR XR-4	-30.4	0	0.9	0.34	-	0.63
Gal Cen	-28.9	0	0.9	0.34	0.95 B	0.65
GX1+4	-24.7	0	0.9	0.36	-	0.67
Kep1604	-21.5	2	0.9	1.12	-	2.12
GX9+9	-17.0	0	0.9	0.40	-	0.75
Sco XR-1	-15.6	1	0.9	0.85	1.5 B	1.59
Aquarius	-1.0	4	0.8	2.48	-	4.66
4U0336+01	0.6	1	0.8	1.17	-	2.19
AQL XR-1	0.6	0	0.8	0.57	-	1.18
2U1907+2	1.3	0	0.8	0.58	-	1.27
SER XR-1	5.0	0	0.7	0.67	-	1.41

Table 3—Continued

Source	δ (degrees)	Events in 3°	Backg. in 3°	ν induced μ-Flux Limits (10^{-14} cm^{-2} s^{-1})	Previous best μ limits (10^{-14} cm^{-2} s^{-1})	ν-Flux limits (10^{-6} cm^{-2} s^{-1})
SS433	5.7	0	0.7	0.67	1.8 B	1.27
2U0613+09	9.1	1	0.6	1.52	-	3.02
Geminga	18.3	0	0.5	1.12	3.1 I	2.10
Crab	22.0	1	0.4	2.52	2.6 B	4.70
2U0352+30	31.0	2	0.3	5.98	-	11.43
Cyg XR-1	35.2	0	0.2	3.24	-	6.24
Her X-1	35.4	0	0.2	3.30	4.3 I	6.96
Cyg XR-2	38.3	0	0.1	4.99	-	10.61
MRK 421	38.4	0	0.1	5.00	3.3 I	9.56
MKN 501	40.3	0	0.1	5.73	-	10.69
Cyg X-3	40.9	0	0.1	6.59	4.1 I	12.49
Per XR-1	41.5	0	0.1	7.51	-	13.99

Wimps (neutralinos)

several·10 $\lesssim m \lesssim$ several·100 GeV

Dark matter (= Wimps) → 地球に捕獲 → 対消滅 → ν

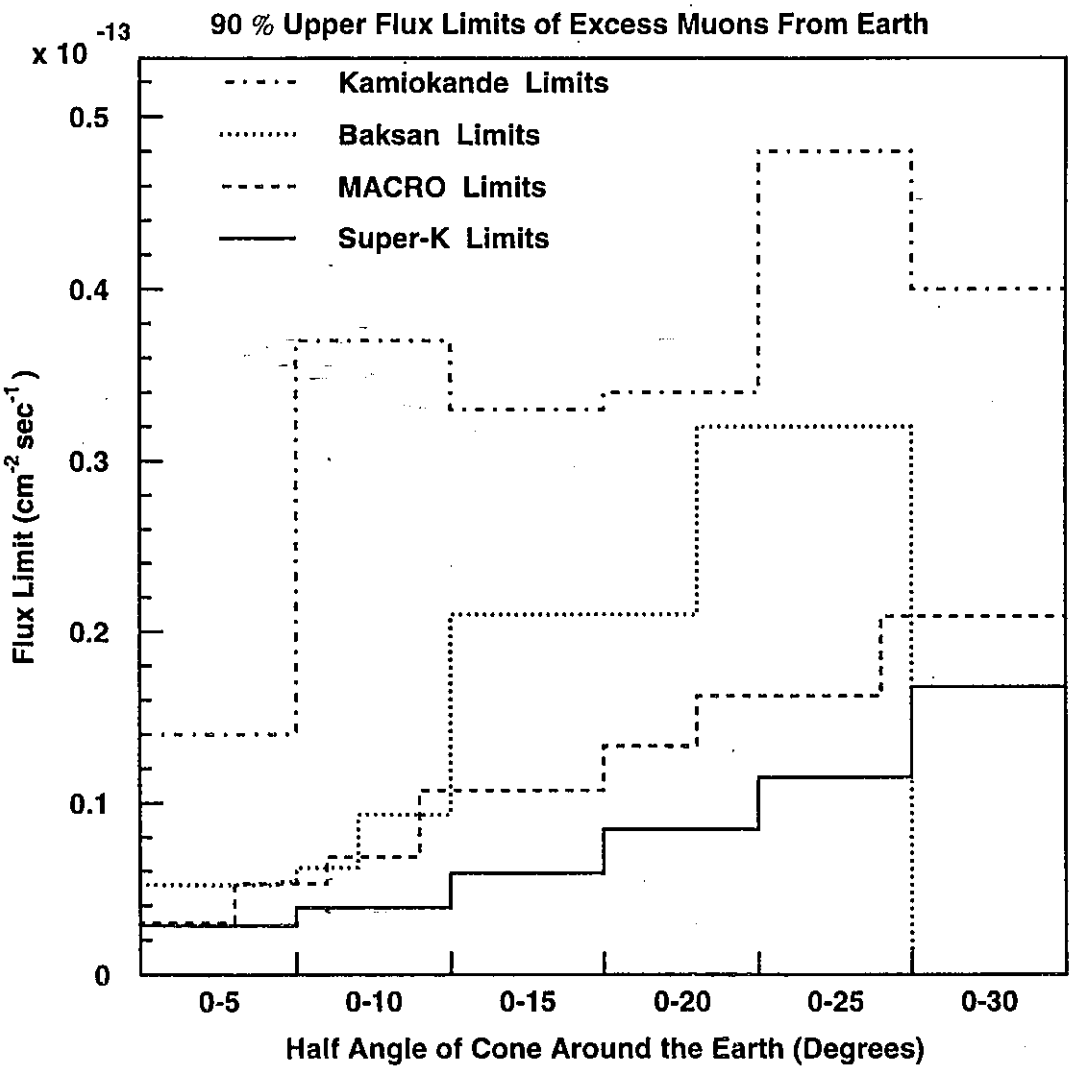

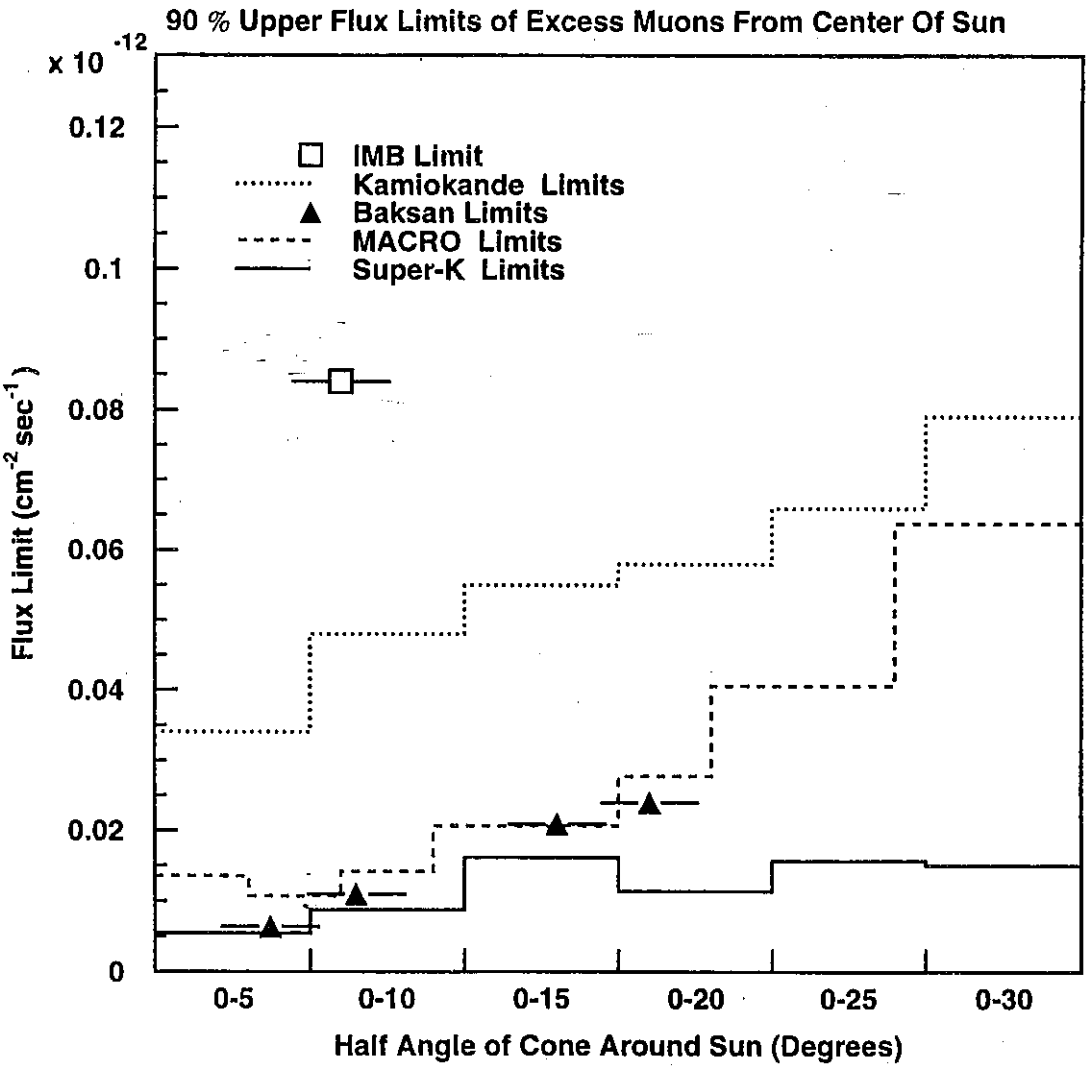
90 % Upper Flux Limits of Excess Muons From Center Of Sun
x 10 -12
0.12
0.1
0.08
0.06
0.04
0.02
0
IMB Limit
Kamiokande Limits
Baksan Limits
MACRO Limits
Super-K Limits
Flux Limit (cm-2 sec-1)
0-5
0-10
0-15
0-20
0-25
0-30
Half Angle of Cone Around Sun (Degrees)

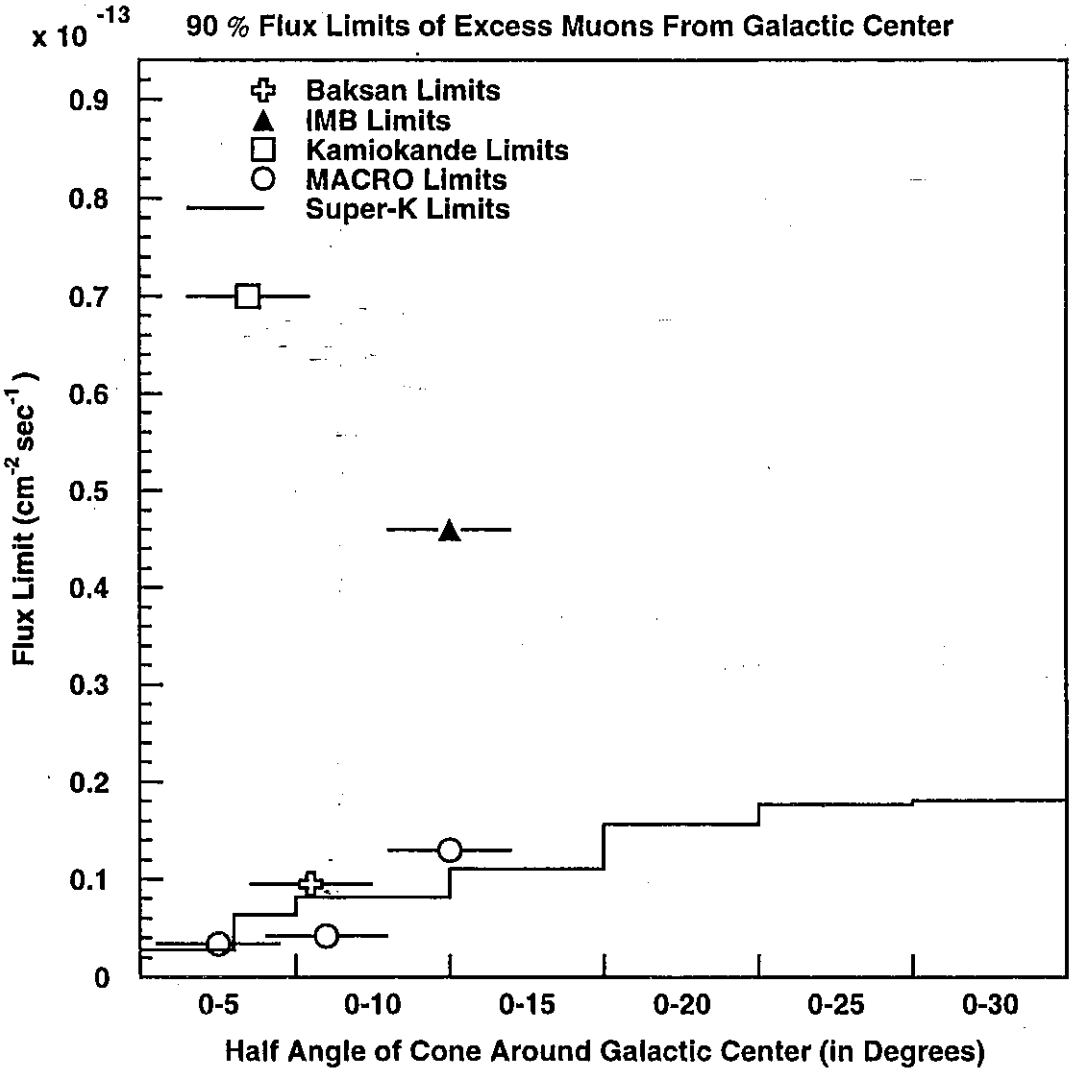
90 % Flux Limits of Excess Muons From Galactic Center
x 10 -13
Baksan Limits
IMB Limits
Kamiokande Limits
MACRO Limits
Super-K Limits
Flux Limit (cm-2 sec-1)
0.9
0.8
0.7
0.6
0.5
0.4
0.3
0.2
0.1
0
0-5
0-10
0-15
0-20
0-25
0-30
Half Angle of Cone Around Galactic Center (in Degrees)

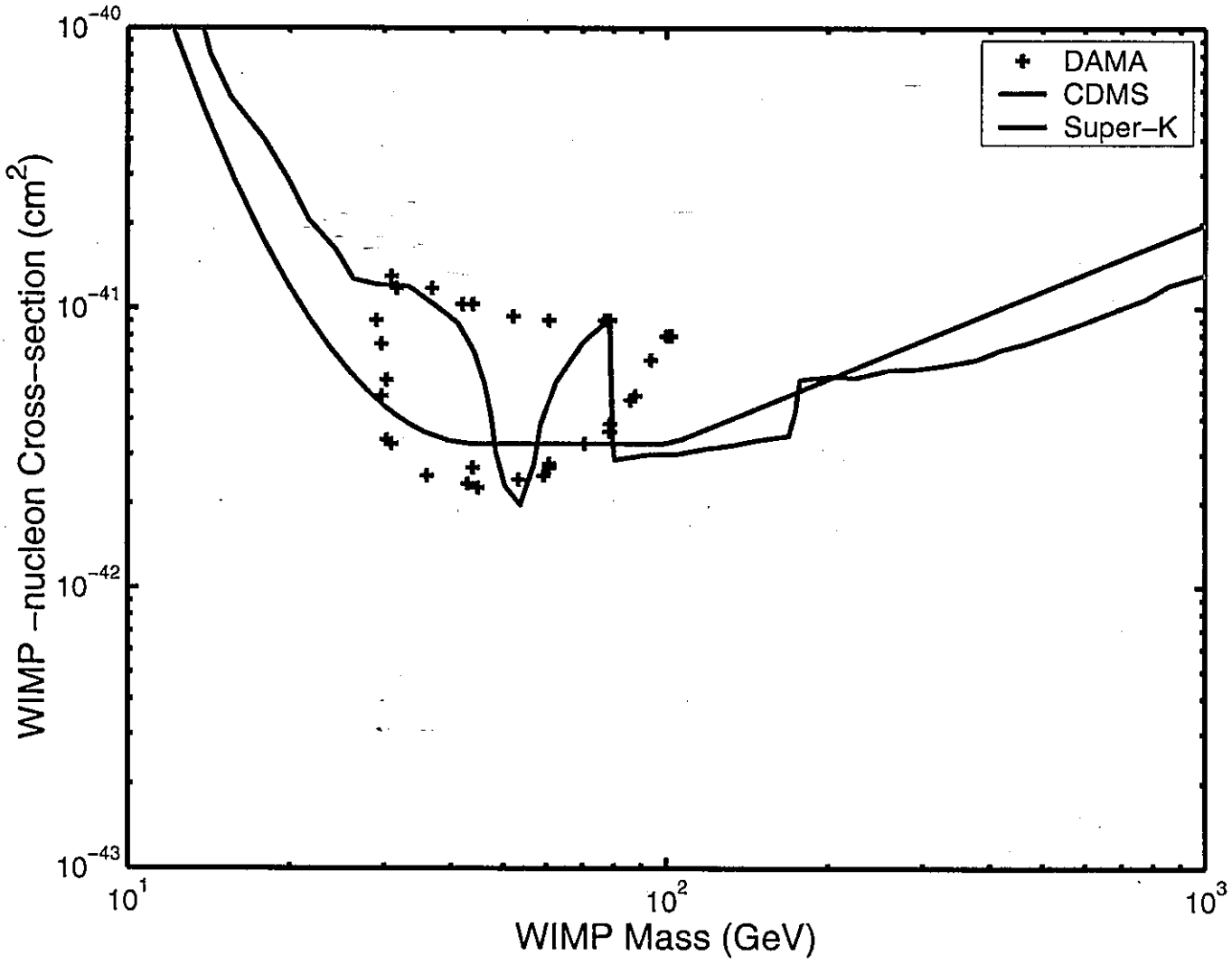
DAMA
CDMS
Super−K
WIMP −nucleon Cross−section (cm^2)
WIMP Mass (GeV)
10^{-40}
10^{-41}
10^{-42}
10^{-43}
10^1
10^2
10^3

SEARCH FOR G.U.T. MAGNETIC MONOPOLES

The MACRO detector, optimized for the search for supermassive ($M > 10^{17}$ GeV) magnetic monopoles (MM) predicted by Grand Unified Theories (GUT) of the electroweak and strong interactions, has a modular structure with three types of detectors: streamer tubes, liquid scintillators and nuclear track detectors which allow redundant informations. No monopole candidate was observed.

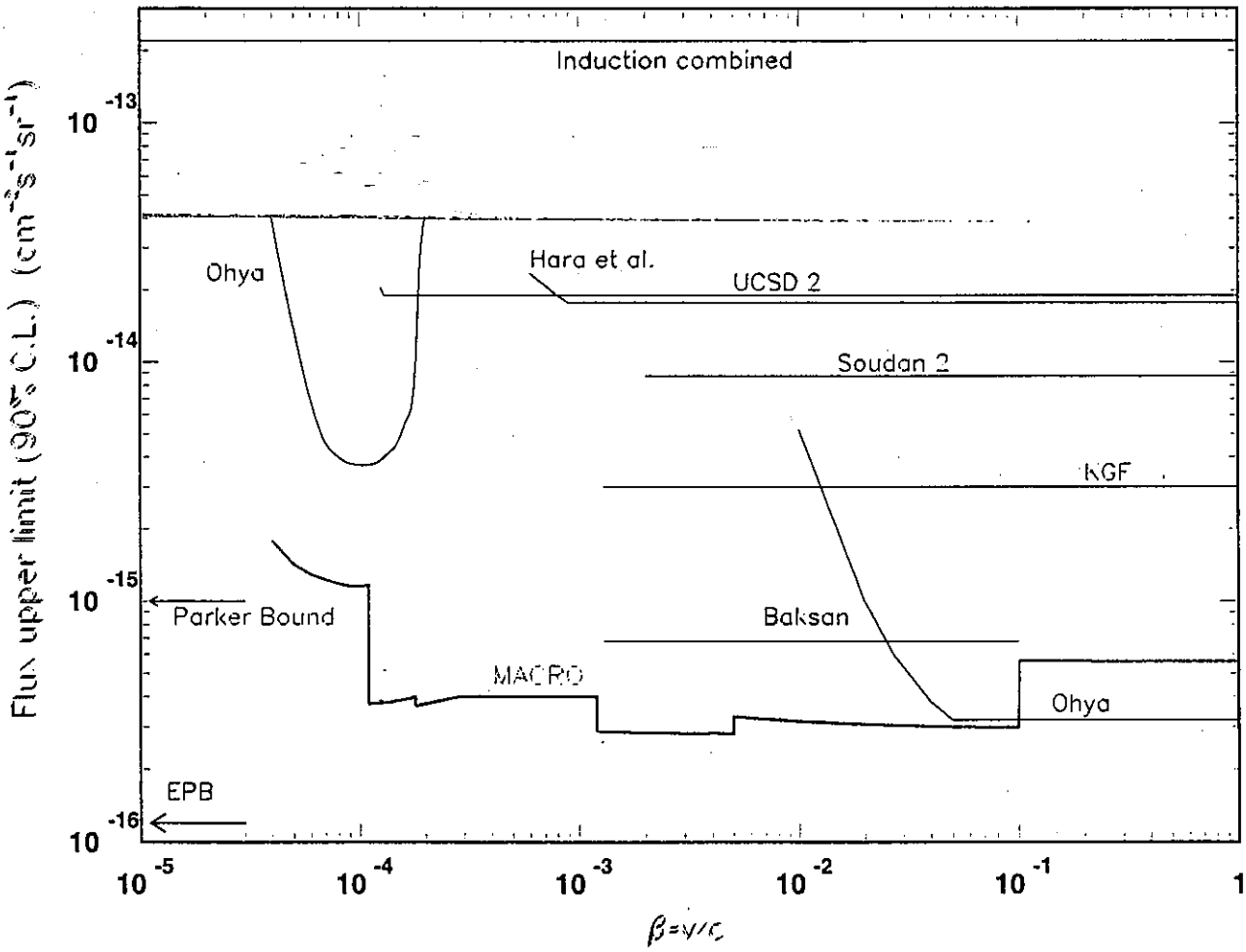

Compilation of upper limits (90% C.L.) for an isotropic flux of MM with $g = g_D$ obtained by MACRO and by other experiments. The global MACRO limit was determined as the OR combination of the separate independent limits from the subdetectors.

Underwater/Underice Detectors

DUMAND	太平洋(ハワイ島沖)		つぶれ
Baikal	バイカル湖	}	運転中
AMANDA	南極氷	}	
NESTOR	エーゲ海	}	準備中
Antares	地中海	}	

なぜ深海？（湖底，南極氷）

- 宇宙線バックグラウンド（μ）が少い．
  $\sim 10^{-4}\ cm^{-2}s^{-1}sr^{-1}$
  （νは下からもやってくる）
- 太陽光はとどかない．→ 装置は open でよい．
- 装置（detector array）の拡張が容易 km^3
- 透明度よい $\sim$ 40m (at 450 nm)
  吸収長
  散乱長 {レーリー / ミー}

ただし、

⊗ バックグラウンド光あり．（K^{40}，生物発光）
  ↗ biofouling
  AMANDA 計画 → 南極氷

⊗ 高い圧力（~500気圧）→ 特殊な技術
  荒い海面 → 設置作業
  NESTOR 計画 → 地中海

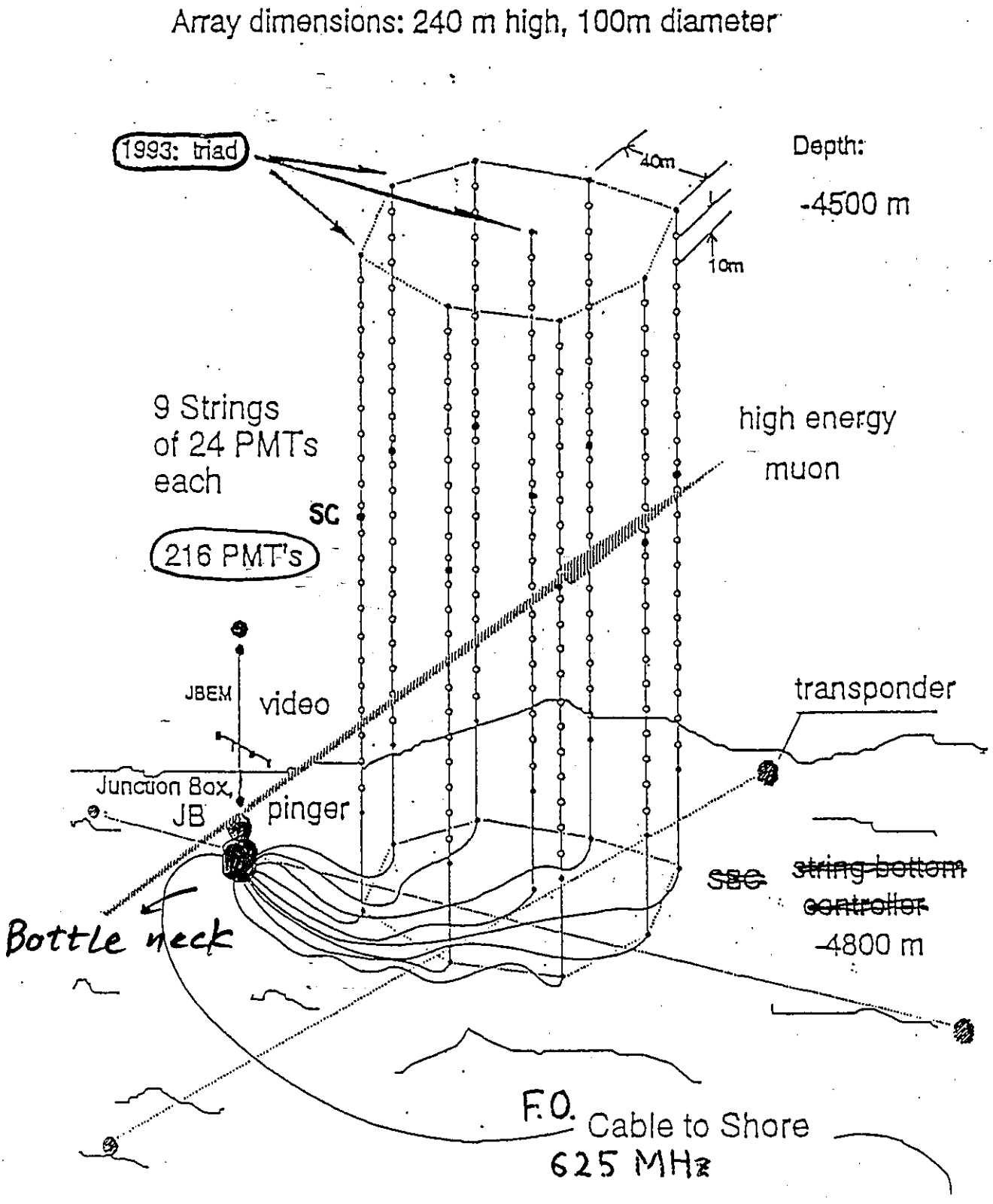

Fig.1 Overall view of DUMAND II

- 海水良
- Bottle neck あり
- 海底山

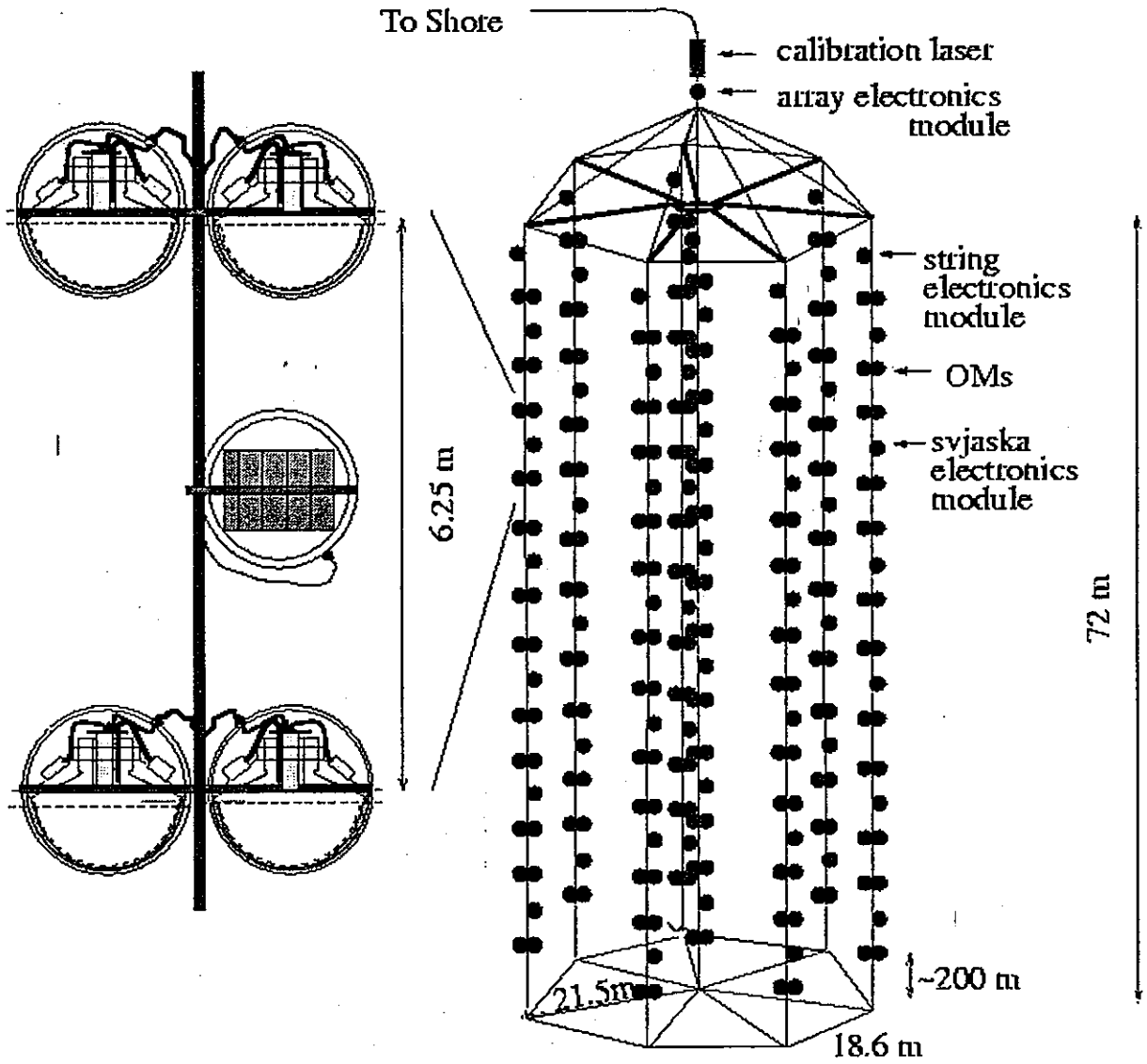

Figure 1: Schematic view of the Baikal neutrino telescope.

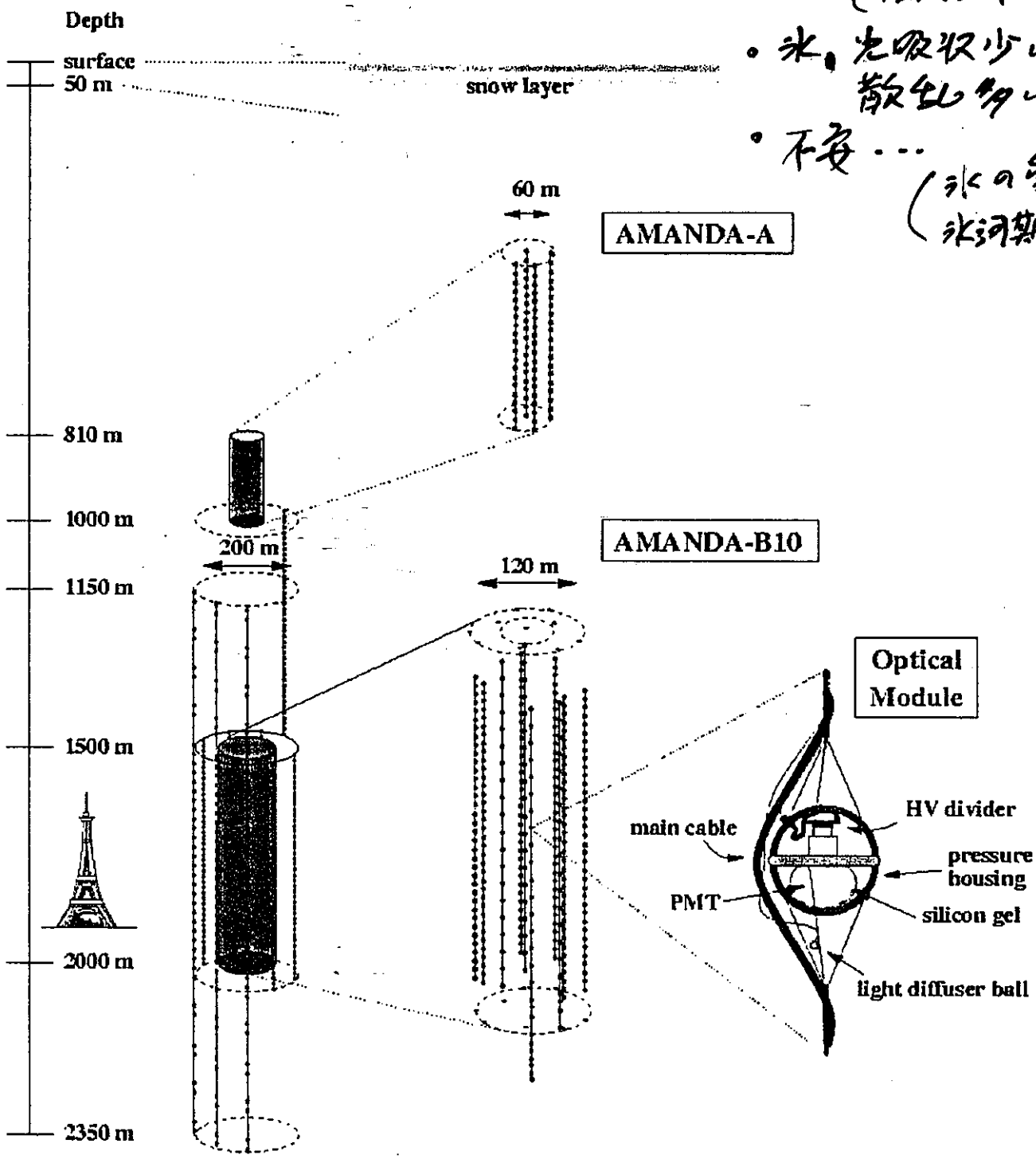

Figure 1: The AMANDA-II array at the South Pole

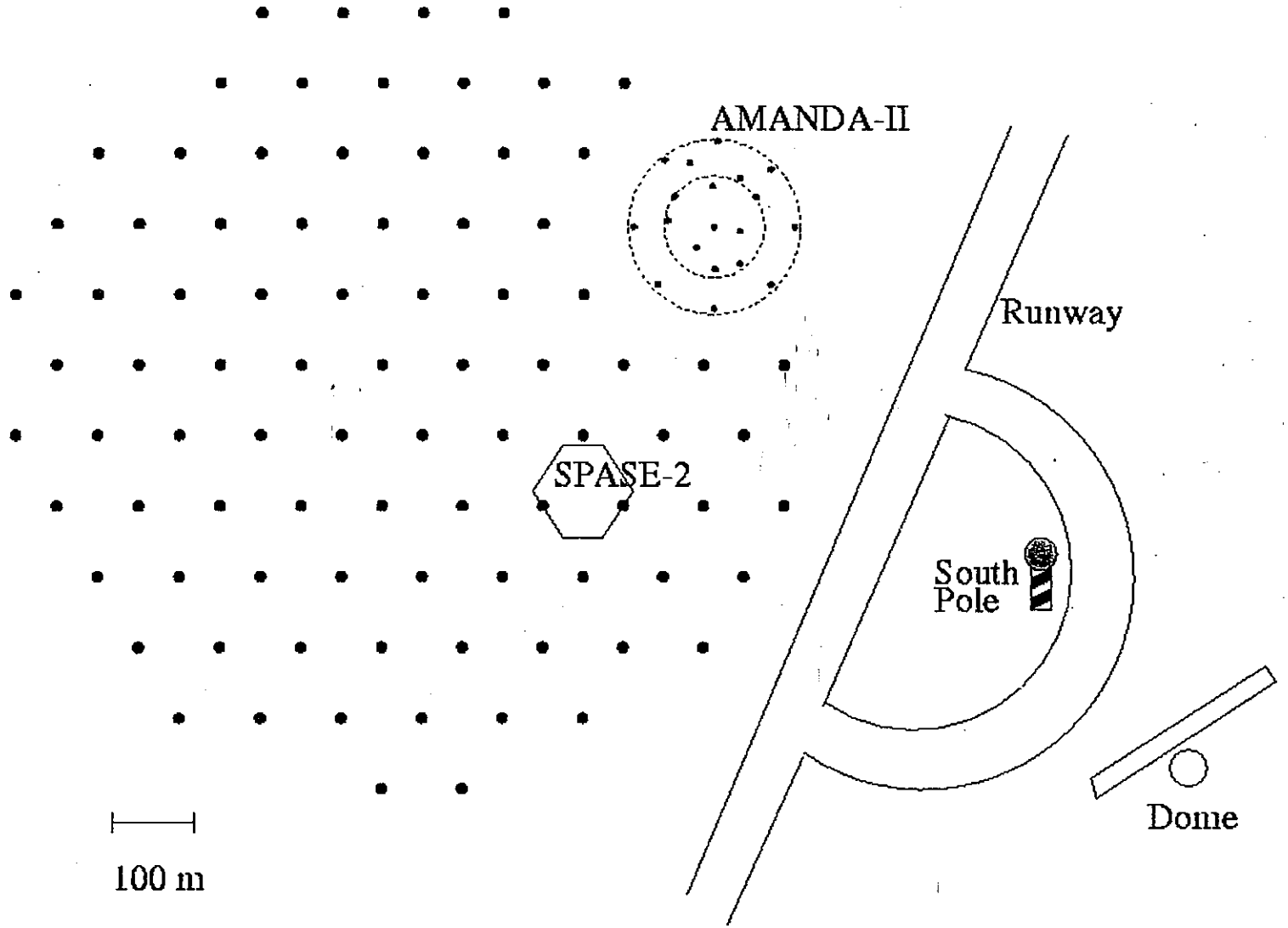

Figure 2. Top view of the proposed ICECUBE detector

NESTOR

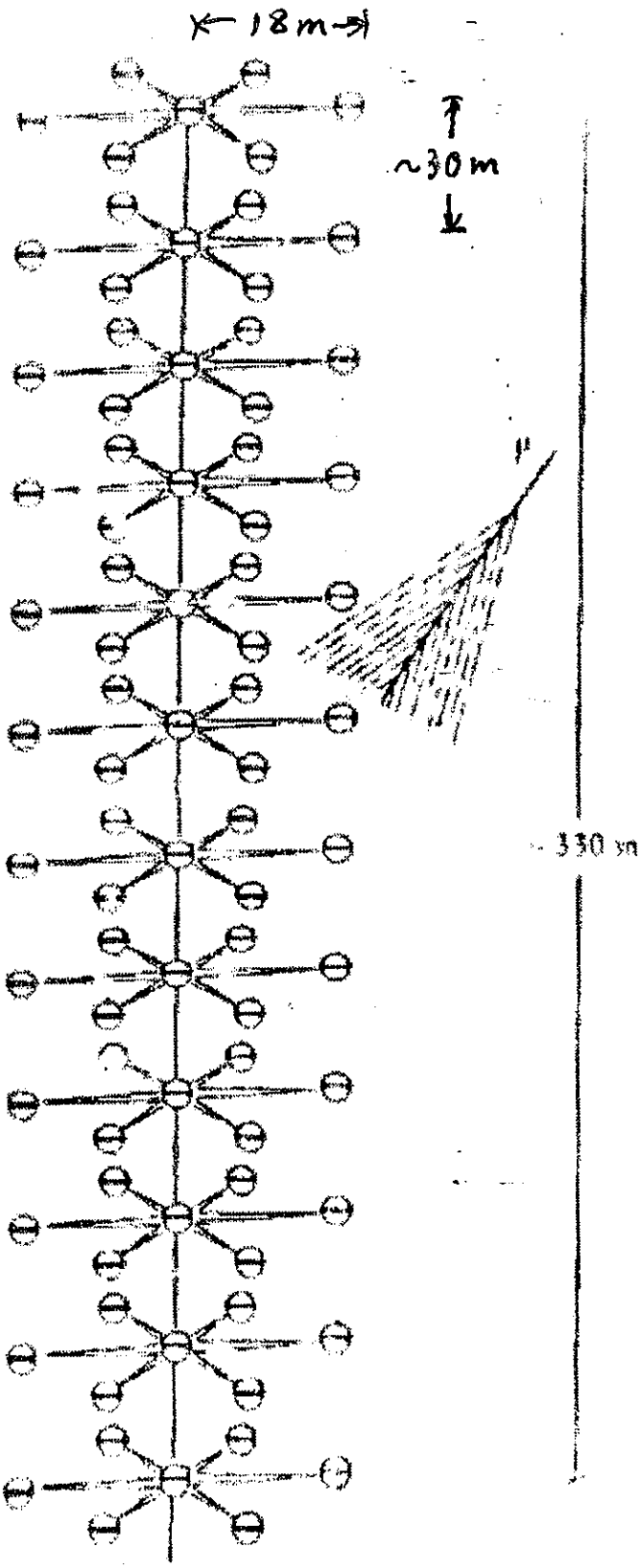

- 場所良
  静かで緑い, 近い
- 海水まあまあ
- デザイン ?? 幅が不足.
  ↳ (方向修正
  先端の速度

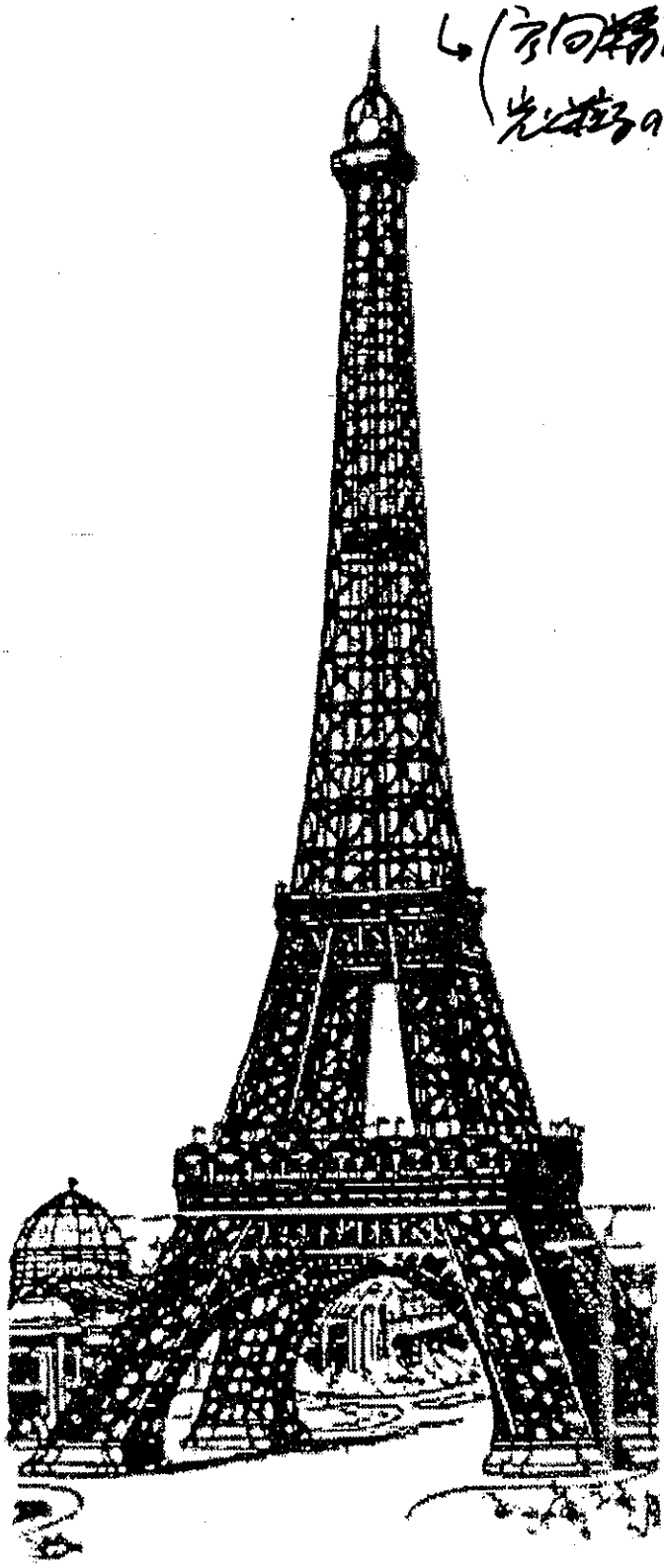

Antares

- インフラ 良
- 海水 悪…
- NESTORの隣りどどきないのか?
- Bottle neck あり.

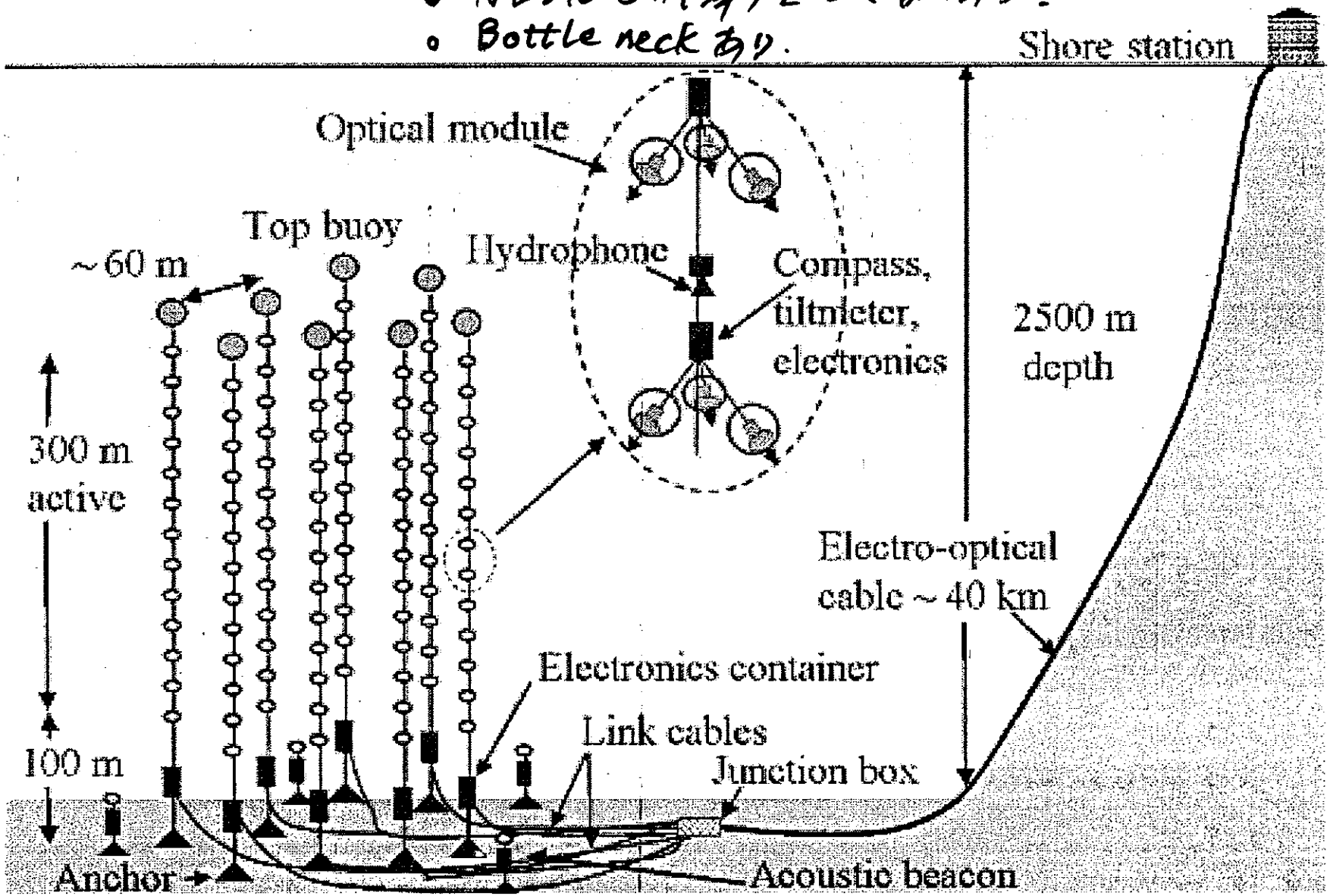

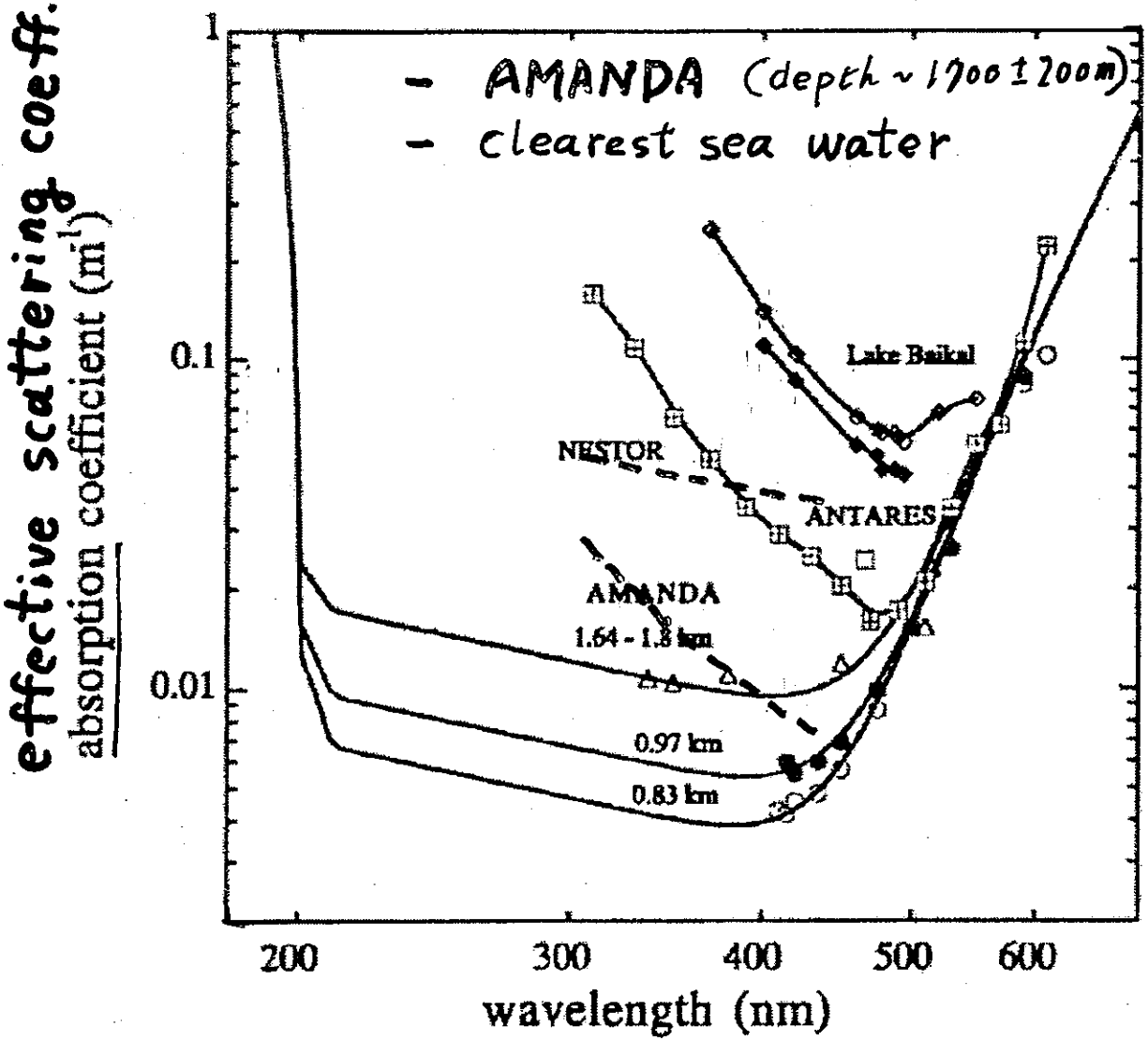

Figure 1. Absorption as a function of wavelength for South Pole ice at depths 0.83 and 0.97 km for AMANDA-A and at 1.64-1.83 km for AMANDA-B, for ocean at the NESTOR and ANTARES sites, and for Lake Baikal. The two sets of data for Baikal illustrate the seasonal variation in absorption (open diamonds for April; closed diamonds for November).

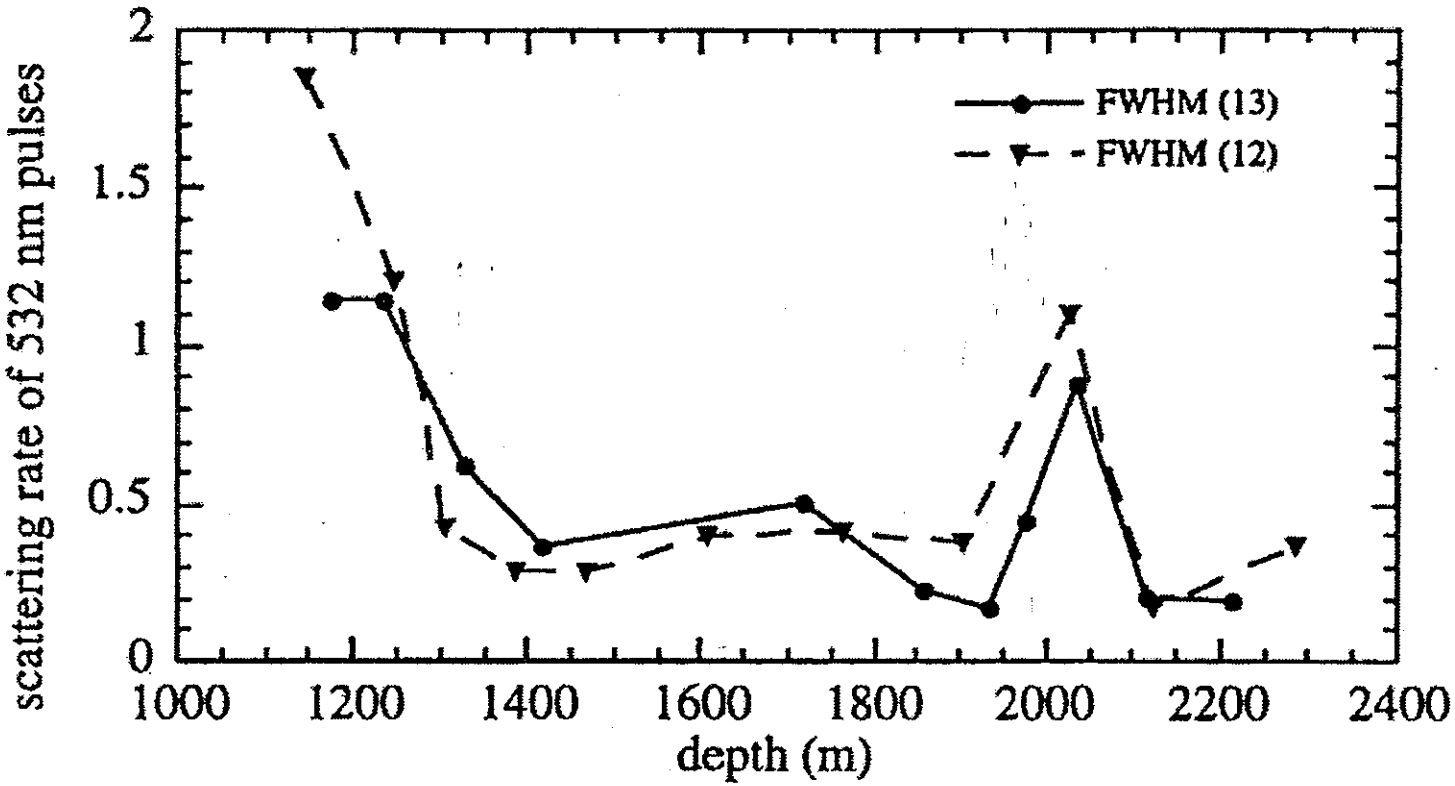

Figure 5. Full Width at Half Maximum of laser timing distributions for pulses from string 13 to 12 (solid circles) and from string 12 to 13 (solid triangles). (Unpublished results of AMANDA collaboration.)

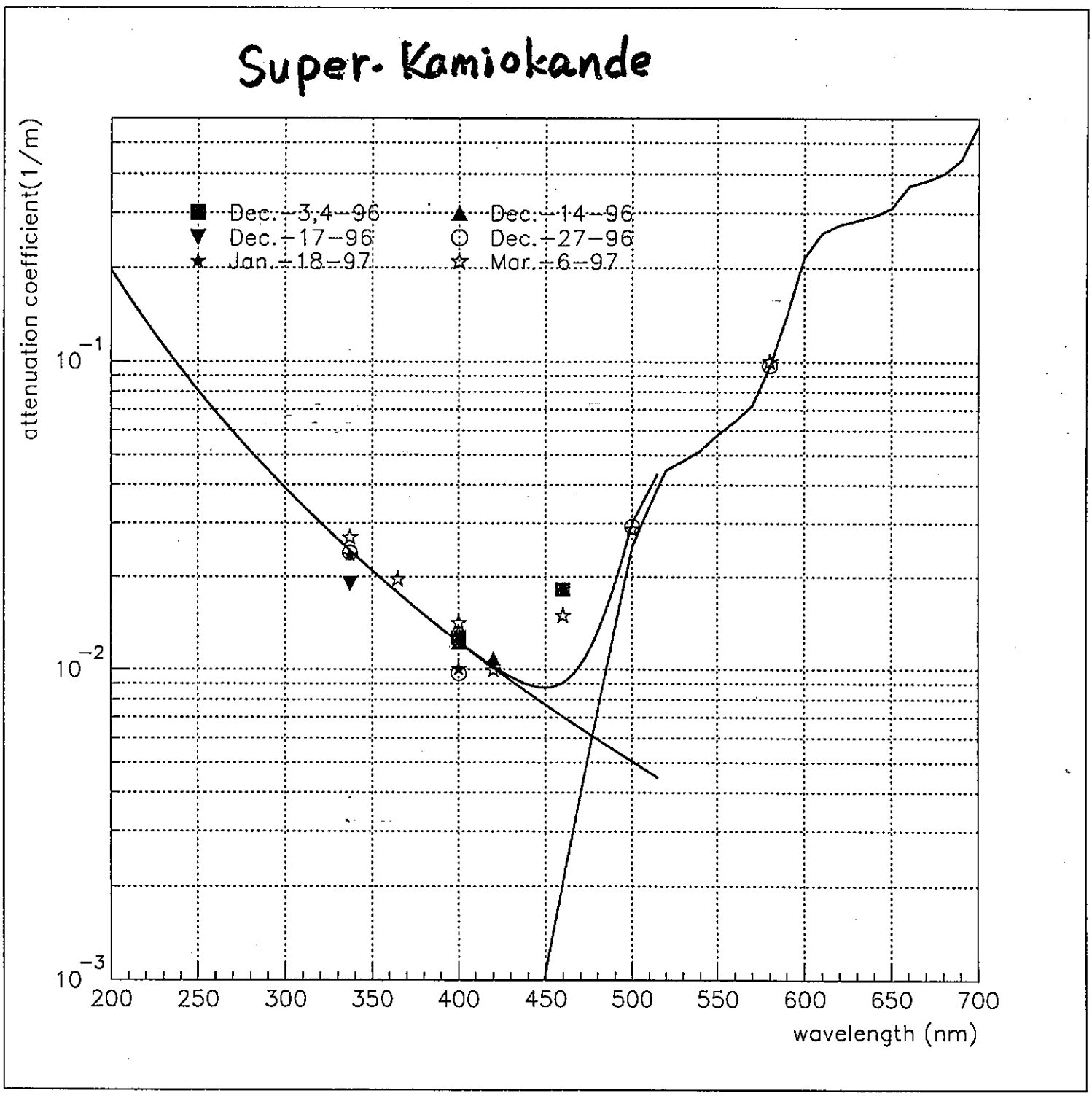
Super-Kamiokande
attenuation coefficient(1/m)
Dec.-3,4-96
Dec.-14-96
Dec.-17-96
Dec.-27-96
Jan.-18-97
Mar.-6-97
10^{-1}
10^{-2}
10^{-3}
200
250
300
350
400
450
500
550
600
650
700
wavelength (nm)

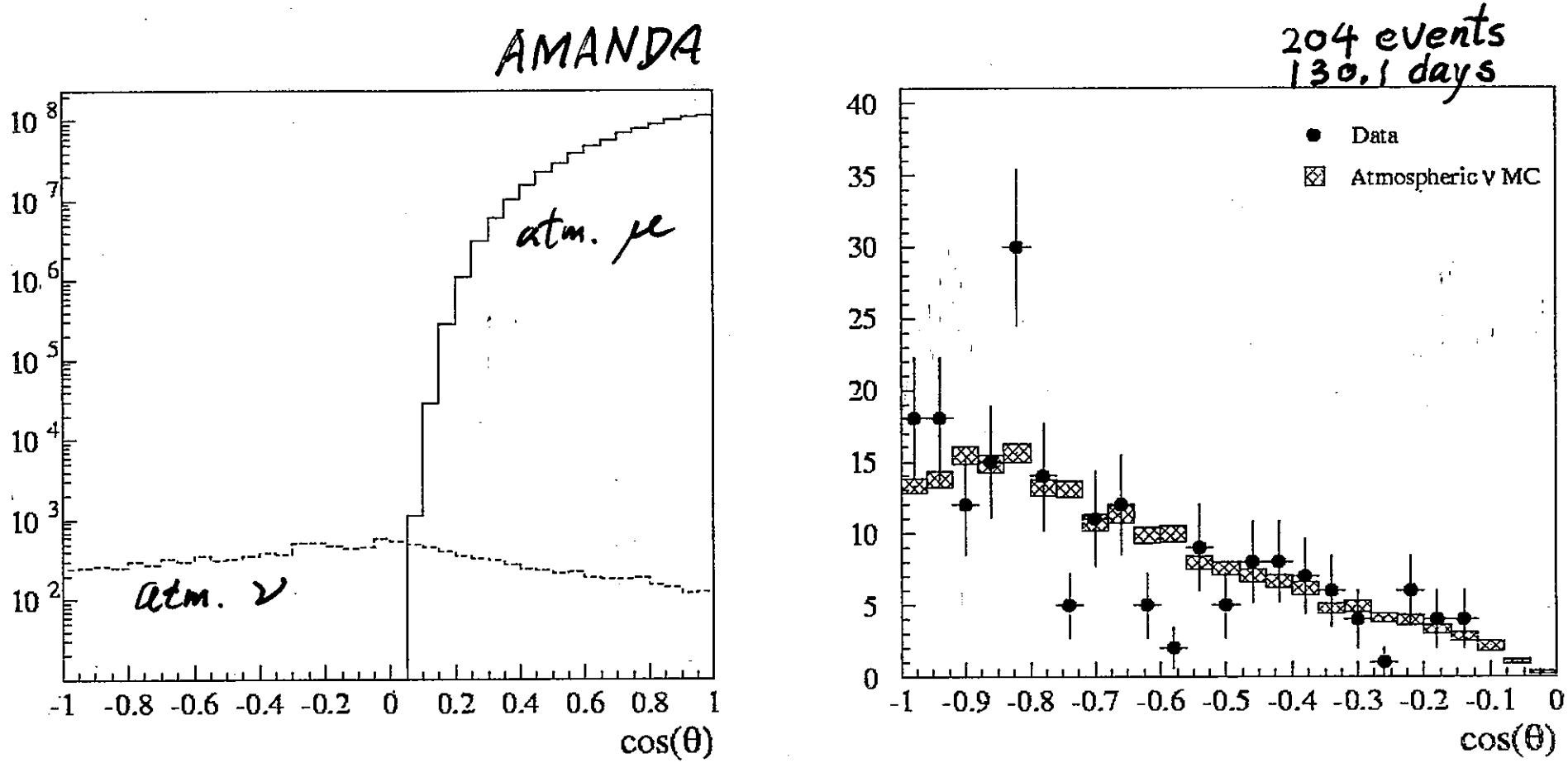

Figure 2: Left: The zenith angle distribution of AMANDA triggers. The solid line represents triggers from downgoing cosmic ray muons. The dashed line shows triggers produced by atmospheric neutrinos. Right: The zenith angle distribution of upward reconstructed events. The size of the hatched boxes indicates the statistical precision of the atmospheric neutrino simulation.

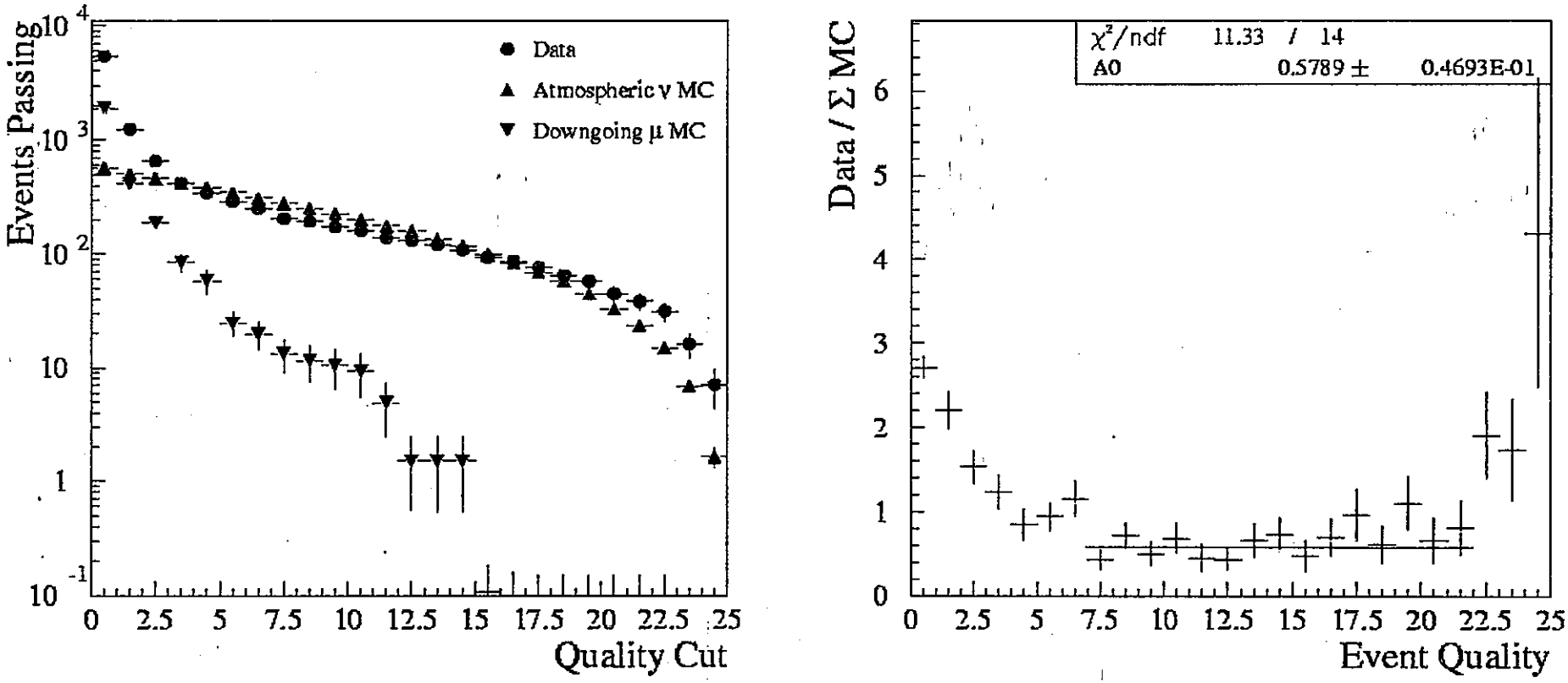

Figure 3: Event quality. Left: Passing rates of events above a certain quality level is shown for background MC, atmospheric neutrino MC and experimental data. Right: Differential presentation of the ratio data/MC.

AMANDA

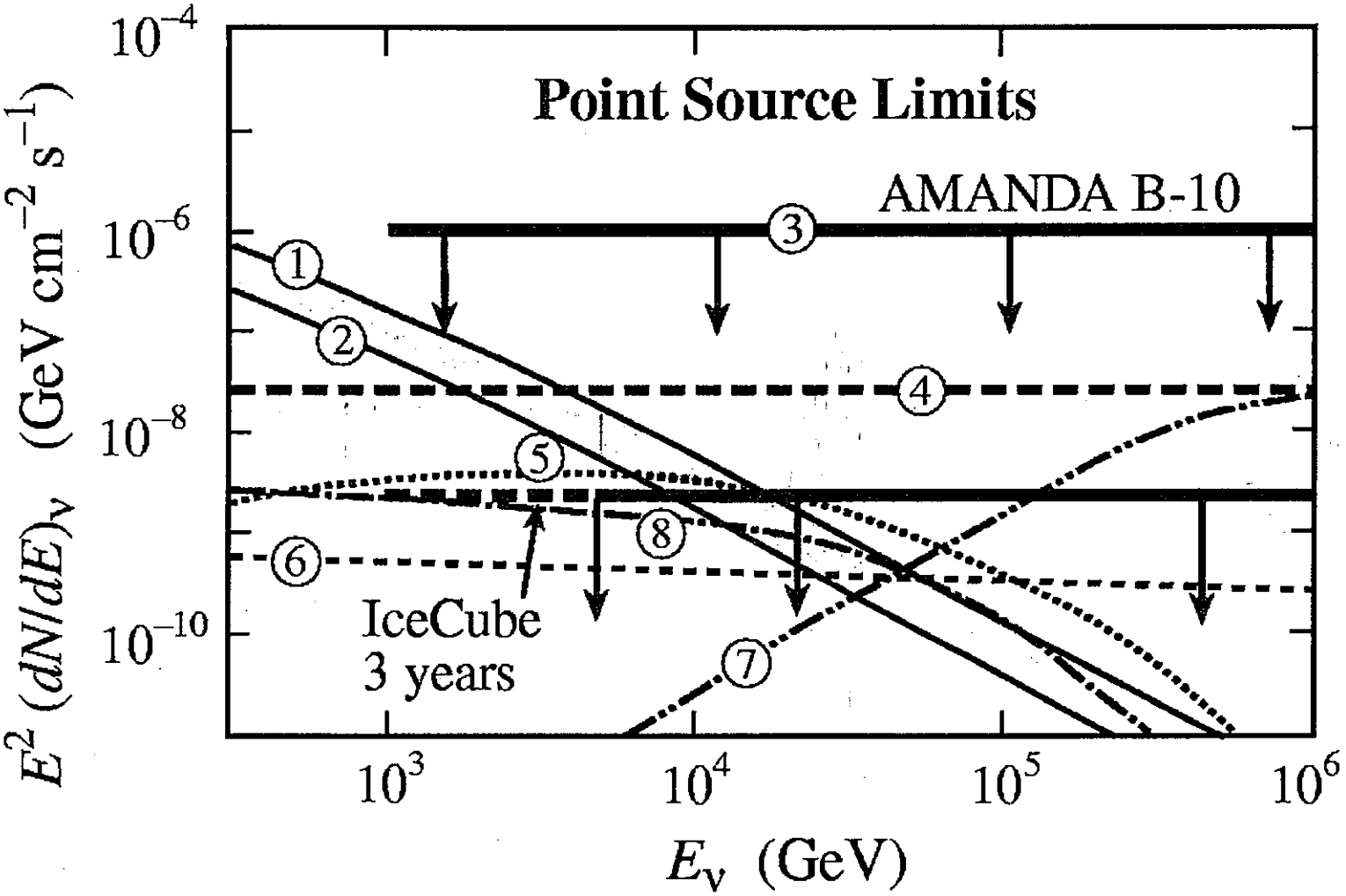

Figure 6: Predictions of high energy $\nu_\mu + \bar{\nu}_\mu$ fluxes from astrophysical sources are shown. Also shown are the preliminary average upper limit as obtained with AMANDA-B10 (3), as well as the sensitivity of the proposed IceCube array after three years of operation. The atmospheric neutrino flux[7] in 2 x 2 degree bin is given as reference: (1) horizontal, (2) vertical. Models: (4) 3C273 pp neutrinos [8], (5) Crab Nebula [9], (6) Coma Cluster [10], (7) 3C273 $p\gamma$ neutrinos [11], (8) Supernova IC443 [12].

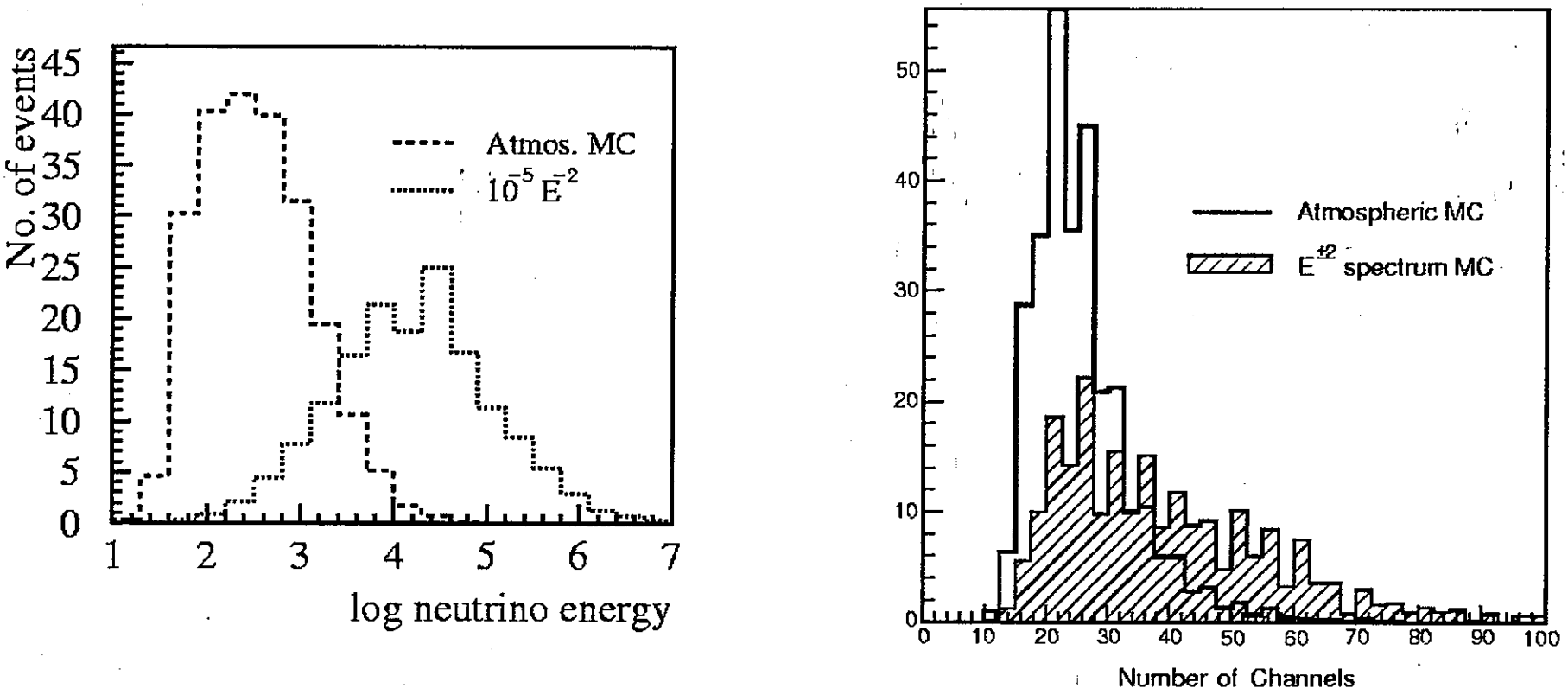

Figure 5: Left: Monte-Carlo simulation of the energy spectrum of atmospheric neutrinos shown in the skyplot in figure reffig:sky. Also shown is the energy spectrum of neutrinos generated by a neutrino flux of a E_ν^{-2}-type energy spectrum (see text).

Data ? preliminary upper limit $\frac{dN}{dE_\nu} \approx 10^{-6} E_\nu^{-2}$ /cm².s.sr.GeV

AMANDA

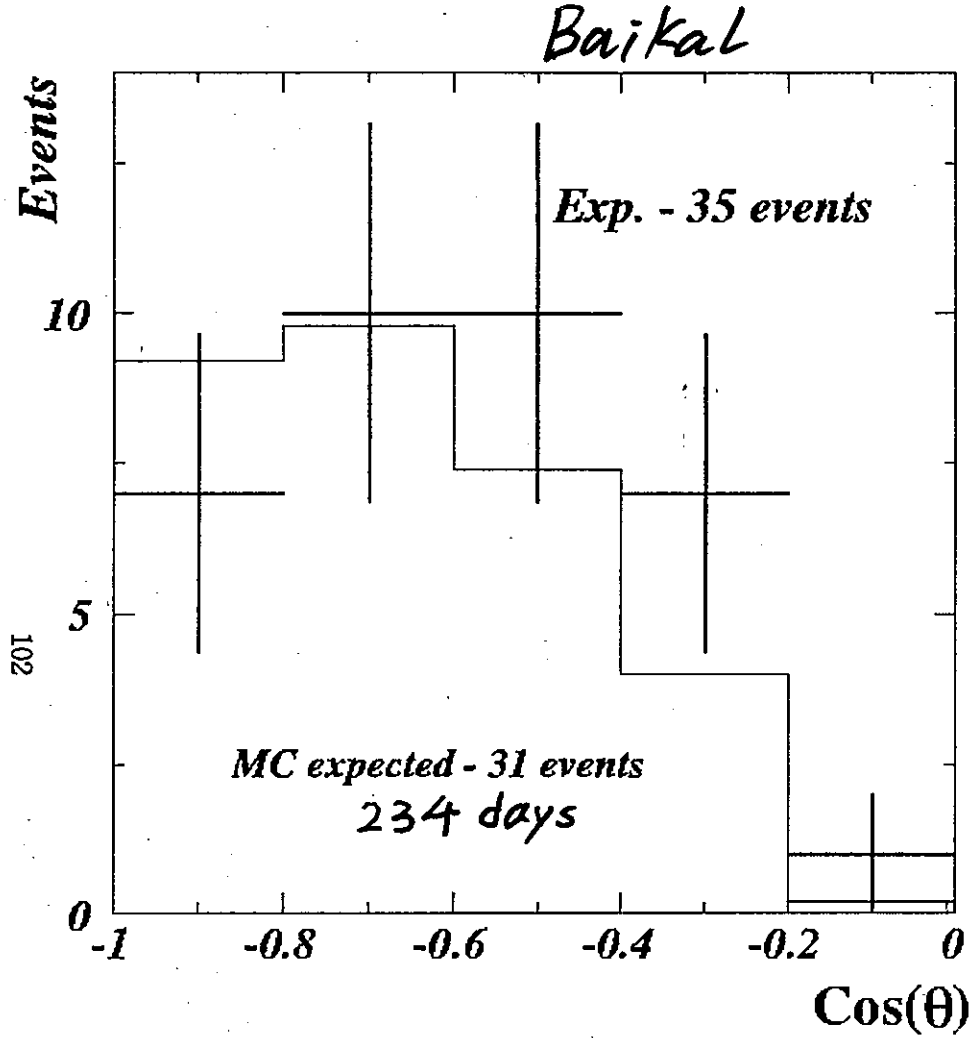

Figure 1. Experimental angular distribution of reconstructed upward going muons in *NT-200*. Filled histogram - MC expected distribution.

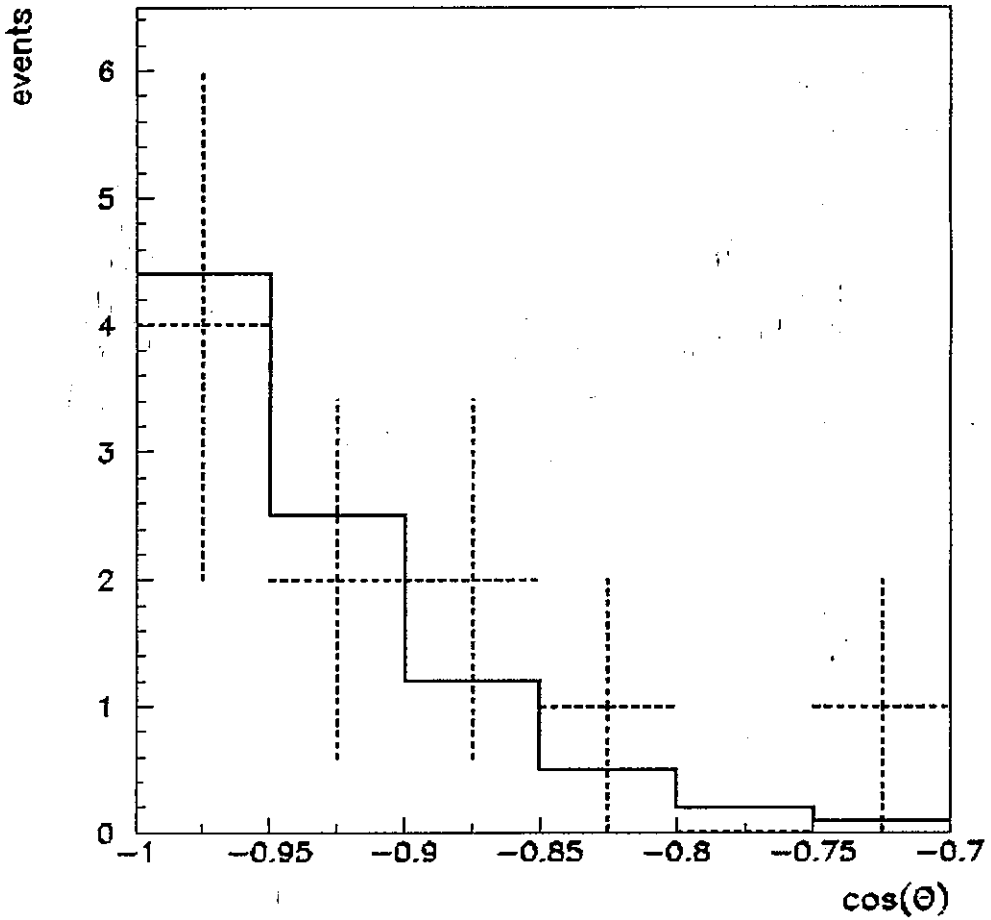

Figure 2. Zenith angular distribution of nearly vertically upward neutrino candidates as well as MC expectation for atmospheric neutrino-induced muons (histogram).

Baikal event selection

For *NT-200* neutrino search, the following cuts are most effective: (1) a traditional χ^2_t cut; (2) the minimum track length in the array; (3) the probability of non-fired channels not to be hit and fired channels to be hit; (4) the correlation of measured amplitudes to the amplitudes expected for reconstructed track; (5) an amplitude χ^2_a defined similar to the time χ^2_t; (6) the correlation between measured hit times and vertical distances of channels in array (see eq.1 below).

耶魔 { Noises
Muon brems.

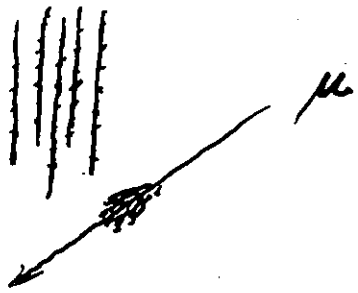

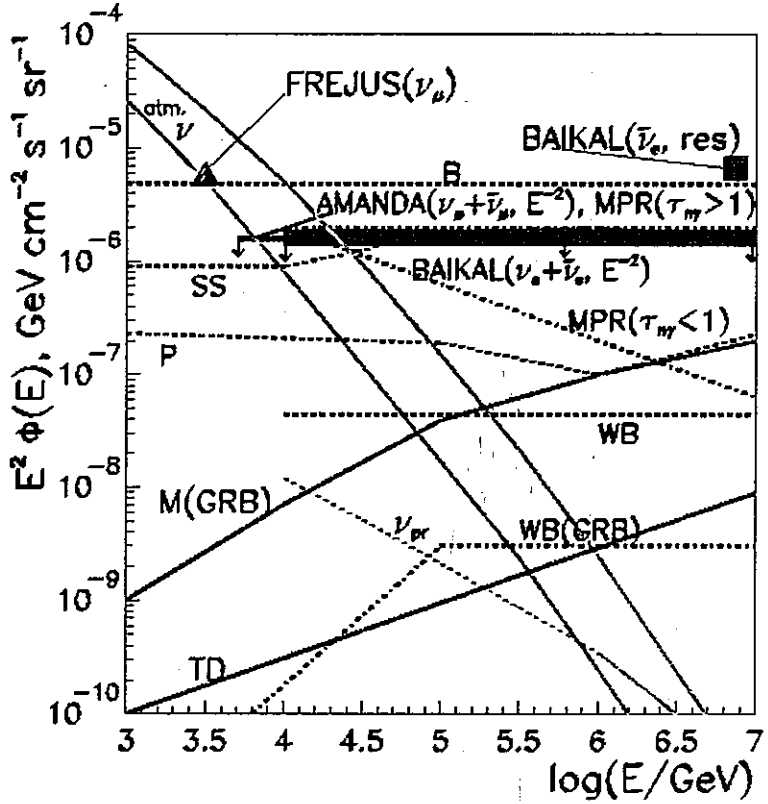

Figure 7: The upper limits on the diffuse neutrino fluxes, obtained by BAIKAL (this work: for E^{-2} flux as well as for a model independent $\tilde{\nu_e}$ flux at resonant energy $6.3 \cdot 10^6$GeV (rectangle)), AMANDA and FREJUS (triangle) experiments as well as the atmospheric conventional neutrino fluxes from horizontal and vertical directions (upper and lower curves, respectively) and atmospheric prompt neutrino flux (curve labeled ν_{pr}). The limits and predictions from different models of high energy neutrino sources are also shown. Curves labeled 'B', 'MPR' and 'WB' represent the model independent limit derived by Berezinsky and the upper bounds derived by Mannheim et al. as well as by Waxman and Bahcall. Curves labeled as 'SS' and 'P' show predicted fluxes from quasar cores and Protheroe respectively. Curves labeled 'M(GRB)' and 'WB(GRB)' represent predicted fluxes from GRBs derived by Mannheim and Waxman and Bahcall. Curve labeled 'TD' - prediction for neutrino flux from topological defects due to specific top-down scenario BHS1.

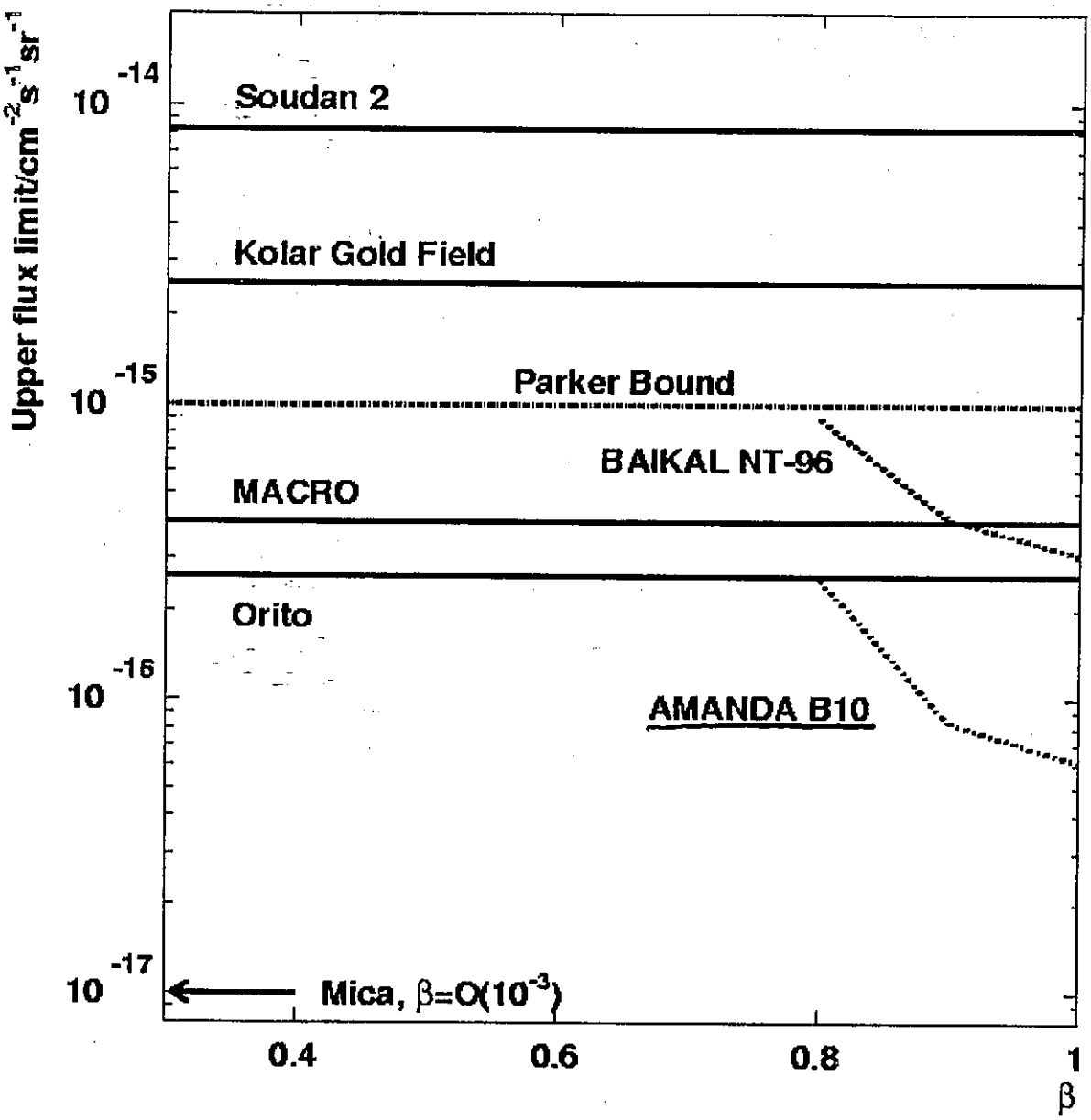

Fig. 4. Flux limits (90% C.L.) for relativistic monopoles gained from various experiments (Cei et al. , 1998). The BAIKAL result (Domogatsky et al., 2000) is based on $T \times \eta$=72 days live time.

他の研究テーマとして.

GRB
SN
WIMP
:

Concluding remark

- 現 AMANDA は HE μ ($E_\mu \gtrsim 1$ TeV) に対しては Super-Kamiokande の 10 倍以上の有効面積があるらしい。
- 2", km^3 ICECUBE は実現するのではないか。
- 問題は、HE (or UHE) ν が十分にやって来るかどうか？